

Persistence and Robustness of Lagrangian Coherent Structures

Uncertainties in the Finite Time Lyapunov Exponent in an ocean ensemble prediction model

Mateusz Matuszak¹, Johannes Röhrs¹, Pål Erik Isachsen^{1,2}, and Martina Idžanović¹

¹Norwegian Meteorological Institute, Henrik Mohns Plass 1, 0371 Oslo, Norway

²Department of Geosciences, University of Oslo, P.O. Box 1022, Blindern, 0315 Oslo, Norway

Correspondence: Mateusz Matuszak (mateuszm@met.no)

Abstract. Lagrangian coherent structures (LCS) are transient features in ocean circulation that describe particle transport, revealing information about transport barriers and accumulation or dispersion regions. ~~Various methods exist to infer LCS from surface current fields provided by ocean circulation models~~ Finite time Lyapunov exponents (FTLE) approximate LCSs under certain conditions, and are here used to characterize flow field features and their uncertainties in predictions from a regional ocean forecast system. Generally, Lagrangian trajectories as well as ~~LCS analysis inherit the~~ FTLE analysis inherit uncertainty from the underlying ocean model, bearing substantial uncertainties as a result of chaotic and turbulent flow fields. In addition, velocity fields and resulting ~~LCS FTLE~~ evolve rapidly. ~~In this study, finite time Lyapunov exponents (FTLE) are used to detect LCSs in surface current predictions from a regional ocean forecast system.~~ We investigate the uncertainty of ~~LCS FTLE fields~~ at any given time using an ensemble prediction system (EPS) to propagate velocity field uncertainty into the ~~LCS analysis.~~ ~~We evaluate variability of FTLE fields~~ FTLE analysis. Variability in time and ~~across the ensemble at fixed times~~ ensemble realisations is evaluated. Averaging over ensemble members can reveal robust FTLE ridges, i.e. FTLE ridges that exist across ensemble realisations. Time averages reveal persistent FTLE ridges, i.e. FTLE ridges that occur over extended periods of time. We find that ~~LCS FTLE features~~ are generally more robust than persistent ~~for the chosen time interval~~. Large scale FTLE ridges are more robust and persistent than small scale FTLE ridges. Averaging of FTLE field is effective at removing chaotic, short-lived and unpredictable structures and may provide the means to employ ~~LCS FTLE~~ analysis in forecasting applications that require to separate uncertain from certain flow features.

1 Introduction

~~Oceanic flows transport various~~ Ocean currents transport and disperse various environmental tracers, such as nutrients, plankton and pollution. ~~The dynamic processes that govern such transport span over several orders of magnitude (Röhrs et al., 2021), and the exact prediction of tracer fate is unfeasible due to the nonlinear chaotic nature of geophysical flow. Low predictability of ocean currents and the associated error propagation into trajectory calculations causes large uncertainties in any tracer transport study and forecast (e.g. Dagestad and Röhrs, 2019).~~

Velocity fields required for ocean transport studies are commonly obtained from Studying and predicting such transport is of interest and importance for environmental management, especially in the coastal zone. Prediction typically relies on the use of Oceanic General Circulation Models (OGCMs). Velocity fields are highly sensitive to small variations in initial conditions, leading to uncertainties in a) the flow field and b) the resulting particle trajectories. This is reflected in numerical analyses, e.g. Lagrangian particle trajectories, which may yield large errors over time due to small errors in initial flow fields, position or time of release.

, in which the nonlinear governing equations of motion are first integrated numerically to determine a velocity field, and where this field is then used to calculate transport and spreading of (synthetic) tracers or particles. In many applications, the aim is not necessarily an exact tracking of individual particles as much as the identification of regions of high or low particle concentration as well as flow features that may act as dynamical barriers between such regions. To this end, the concept of Lagrangian Coherent Structures (LCS) provide a diagnostic description of particle transport in complex dynamical flows independent of individual trajectories. Proposed by Haller and Yuan (2000), LCSs identify time-evolving shapes has received increased attention from the oceanographic community. As the name suggests, LCSs are coherently evolving features in unsteady and chaotic flow fields like eddies or jets, which influence trajectory patterns. Hyperbolic LCSs characterize attraction and repulsion in the flow, whereas parabolic and elliptic LCSs describe trajectories in jets and vortex boundaries (Haller, 2015). In two-dimensional (2D) flows, hyperbolic LCSs manifest as one-dimensional (1D) curves, locally acting as the most attracting or repelling structures over a time interval. A key trait of hyperbolic LCSs is their role as effective transport barriers; material converges towards or diverges away from the LCSs without passing through them (e.g., Haller and Yuan, 2000; Lekien et al., 2005; Dong et al., 2021). LCSs yield information about the flow field itself, in particular how the flow field organizes particles and where these are likely to be located. An application of LCS analysis in emergency response that can systematically influence particle trajectories (Haller and Yuan, 2000; Tang et al., 2010; Farazmand and Haller, 2012; Haller, 2015). More specifically, LCSs describe coherent morphological features of the flow field that cause accumulation, spreading and deformation, and they can even suggest the presence of transport barriers. LCSs have therefore found applications in both process studies and emergency responses, e.g. man-over-board scenarios and oil-spill clean-up operations, has since been discussed (e.g. Olascoaga and Haller, 2012; Peacock and Haller, 2013; Dong et al., 2021).

Previous studies often discuss the LCS methodology and their practical applications, but rarely touch upon the topic of LCS estimates being inherently affected by uncertainties in the velocity fields they aim to describe. Furthermore, short-lived flow features constantly develop, drift, and dissipate in real oceanic flow (Chen and Han, 2019). Given their time-dependency, LCSs might appear and disappear just as quickly. This brings up two important questions: (1) Given the velocity field uncertainty, how *robust*, i. e. predictable, are LCSs derived from ocean models at a particular time?; (2) Given their time-dependency, how *persistent* are LCS in ephemeral flows?

Dong et al. (2021) investigated the persistence of a transport barrier, detected as an LCS in the Lofoten-Vesterålen (LoVe) region. The authors identify that the barrier emerges each April for the years considered (2010-2019) and persists for 49 days on average. A low resolution satellite altimetry product was used, which does not capture small-scale or short-lived structures. Nevertheless,

the considered LCS was persistent for a limited time. In another recent study, Badza et al. (2023) investigate the effect of flow-field uncertainty on LCS computations in the Gul Stream, showing that different LCS detection methods respond differently to flow-field uncertainty, arguing a non-robust method is not reliable. However, Various methods have been proposed to find LCSs in observed or modeled velocity fields (e.g. d'Ovidio et al., 2004; Shadden et al., 2005; Haller, 2011; Duran et al., 2018). Among those, the authors do not go into detail as to which underlying dynamics cause robustness in LCSs. Finite-Time Lyapunov Exponent (FTLE) presents an approximation of LCS that is objective and straightforward to apply (Hadjighasem et al., 2017), and is capable of highlighting areas of particle accumulation or spreading—depending on whether it is computed forward or backward in time—for the spatial and temporal scales on which coastal ocean surface flow varies (e.g. Giudici et al., 2021; Ghosh et al., 2022). More specifically, the FTLE describes the stretching that a fluid parcel at a given location experiences over a finite time due to the spatially and temporally-varying velocity field. Elongated patches of elevated FTLE values—hereafter referred to as FTLE ridges—may be interpreted as boundaries between coherent structures (flow features identifiable due to their longevity compared to other nearby flows), that is, boundaries between flow features such as eddies, vortices or meandering jets; and it is near such boundaries that a fluid parcel's motion will change drastically (Hussain, 1983; Samelson, 2013; Balasuriya et al., 2016). In unstable flows, FTLE ridges define time-varying regions exhibiting either an attraction to or repulsion from hyperbolic trajectories (Shadden et al., 2005; Lee et al., 2007; Brunton and Rowley, 2010; Balasuriya, 2012; Balasuriya et al., 2016; van Sebille et al., 2016). Under certain conditions, these FTLE ridges may reveal LCSs (Farazmand and Haller, 2012) and provide a diagnostic tool for describing fluid flows that is pertinent to applications of particle transport.

Here, we elaborate on the idea that LCS analysis could reveal flow-field structures in the presence of uncertainty in the used ocean model. Uncertainty in circulation forecasts are typically quantified by running ensemble simulations with perturbed initial conditions. Using FTLE analysis as a detection for LCS has limitations. For example, a sheared current is not an LCS but will result in high FTLE values, or the detected FTLE ridge may be far away from a true LCS (see example 3 and/or forcing conditions 4 in Haller (2011)). While more complete methods LCS detection exist (e.g. Duran et al., 2018), this article will focus on FTLE analysis since it provides a straightforward gridded spatial description of Lagrangian transport characteristics that can be analyzed using elementary statistical methods. Given its ease of implementation, we ultimately aim to examine the potential use of FTLE analysis as a practical tool for applications in operational oceanography, e.g. oil-spill modeling.

More specifically, the current study will examine the usefulness of an FTLE approach to transport and dispersion modeling in light of the *uncertain* nature of any ocean model forecast. Due to the nonlinear and highly chaotic nature of real ocean flows—as well as the flow in high-resolution ocean models—small errors in the knowledge or specification of the velocity field may yield large perturbations in estimated particle trajectories. Furthermore, even with a perfect knowledge of the velocity field, uncertainties in particle's initial position or time of release may grow into large uncertainties over time. Thus, despite the potential usefulness of LCS or FTLE analysis outlined above, the need to address the uncertainty and errors in e.g. the underlying current velocity remains. Can the uncertainty in forecasted FTLE fields be quantified? A common way to address prediction uncertainties in geophysical flow fields is by use of Ensemble Prediction Systems (EPS). Instead of issuing one single deterministic integration of the circulation model, an ensemble of model realisations is obtained by time-integrating the model with variations in the initial conditions and boundary conditions (e.g. using an ensemble prediction

system (EPS the atmospheric forcing). The aim is that the ensemble spread of circulation realisations represents the ocean state uncertainty (e.g. Sakov et al., 2012; Idžanović et al., 2023). Ensemble members differ by e. g. perturbed initial and boundary conditions, parametrizations, and are initiated based on a probabilistic spread which should be consistent with the model's uncertainty (Leutbecher and Palmer, 2007). Subsequently, an ensemble of trajectory simulations can be based on an OGCM ensemble, such that the spread of trajectories is based on the ensemble is hence intended to span out the possible states of the system (e.g. Lebreton et al., 2012; Idžanović et al., 2023). While common in weather prediction, this method is in its infancy in regional ocean prediction (Thoppil et al., 2021).

The impact of general flow variability on FTLE and other LCS analyses has received some attention, specifically related to the question of whether time-persistent features can be identified in a nonlinear and chaotic flow field (e.g. Olascoaga et al., 2006; Gouveia et al., 2013). There has also been some studies aiming to address uncertainty aspect, using ocean EPSs. (e.g. Wei et al., 2013; Guo et al., 2016; Wei et al., 2017). Here, we wish to further elaborate on how FTLE analysis can give information on coherent flow structures, despite the presence of time variability and uncertainty in the flow field (de Aguiar et al., 2023).

Our study investigates the persistence forecast. We specifically distinguish between *persistence* and *robustness* of LCSs based on a high-resolution ocean EPS in the dynamically active Lofoten-Veseterålen shelfsea region off Northern Norway. *robustness* of flow features: We refer to persistence in relation to flow features that remain at their location over an extended period of time, hence provide usefulness for applications that use an analysis and assume the flow field remains in a similar state. Then we refer to robustness in a prediction of flow features if a majority of a model's ensemble members indicate a similar outcome such that the forecasted FTLE have a high probability to be realized in nature.

Our study region will be the continental shelf, continental slope and deep ocean basin off Lofoten-Veseterålen in Northern Norway, a region of considerable importance for both the marine climate and marine ecosystem in the northern North-Atlantic. In section 2, we describe the ~~used data set from an operational~~ operational EPS ocean forecast system for this region and provide an outline of how the ~~LCS FTLE~~ analysis is performed using ~~Finite-Time Lyapunov Exponents (FTLE)~~. In section 3 we present results invoking time-averages and ensemble averages of FTLE fields, respectively. In section 4, we draw conclusions on temporal and seasonal variability of ~~LCS FTLE~~ and uncertainties in the ~~LCS FTLE~~ analysis. Finally, we discuss implications on the applicability of the ~~LCS FTLE~~ analysis in uncertain flow fields as a tool in operational forecasting.

2 Data and methods

2.1 Study region

The bathymetry and modelled surface currents around Lofoten-Vesterålen (LoVe) archipelago along northern Norway's coast are shown in Figure 1. The continental shelf sea off LoVe is known to be a hot spot for fisheries due to its high concentrations of nutrients, which form feeding grounds and spawning banks for marine life (Sundby and Bratland, 1987; Sundby et al., 2013). Transport of relevant nutrients has been widely studied (e.g. Adlandsvik and Sundby, 1994; Röhrs et al., 2014), and the Finite-Size Lyapunov Exponent (FSLE) analysis presented in Dong et al. (2021) shed light on possible mechanisms for cross-slope transport of nutrients that could play a role in sustaining biological production.

The LoVe region is characterized by complex bottom topography and a steep continental slope that steer the region's primary large-scale currents (Sundby, 1984), namely the Norwegian Atlantic Slope Current (NwASC) (Rossby et al., 2009) and the Norwegian Coastal Current (NCC) (Gascard et al., 2004). The complex coastline and the Vestfjorden embayment directly guide the path of the NCC, and also cause complex flow features, including strong tidal currents through through Moskstraumen—one of the many straits that cut through the archipelago (Børve et al., 2021). During winter, southerly winds enhance the onshore Ekman transport and water mass accumulation along the coast, thus speeding up the large-scale currents after geostrophic adjustment (Mitchelson-Jacob and Sundby, 2001).

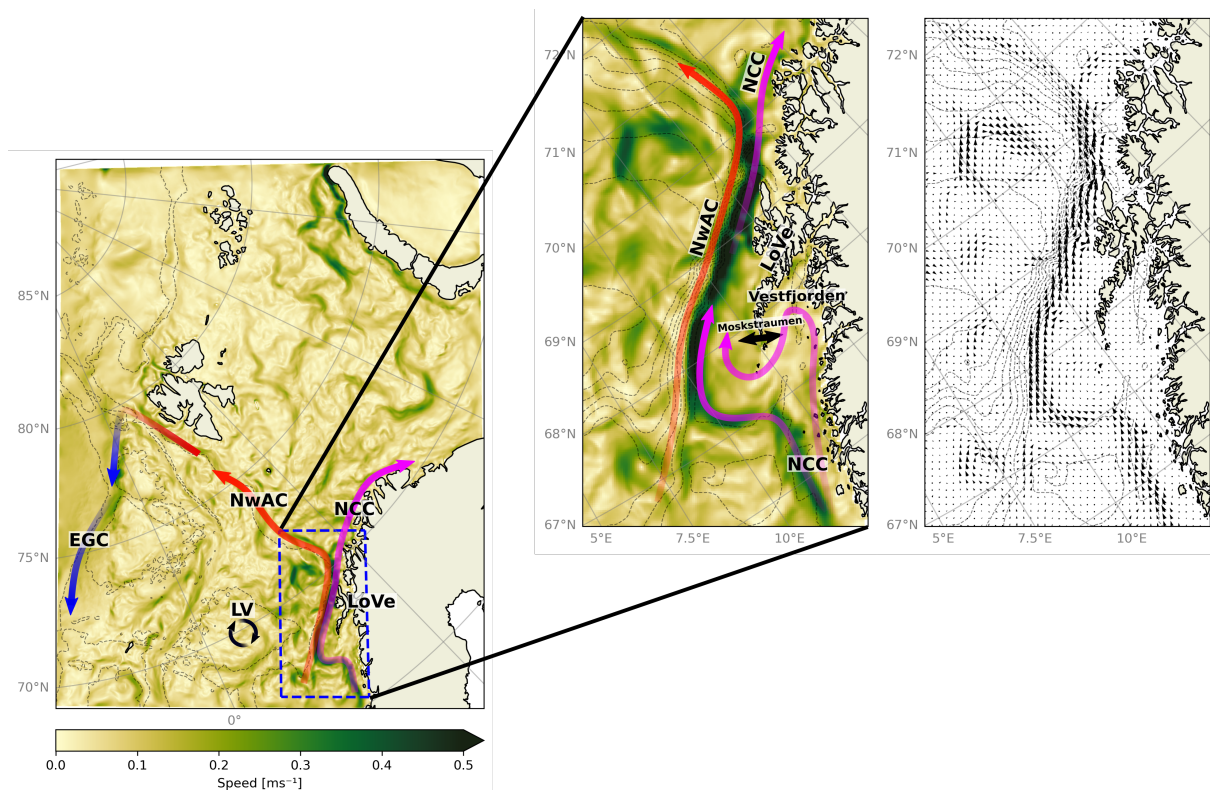


Figure 1. Average ocean current speed [ms^{-1}] for the period 2023-02-01 to 2023-02-28 over the full Barents-2.5 model domain. Dashed blue lines highlight the region of interest for this study, which is the oceanic part around the Lofoten-Vesterålen islands (LoVe) and is enlarged. Arrows in the rightmost panel indicate average current velocities for the period. Bathymetry is indicated by gray dashed lines. Purple arrows indicate the Norwegian Coastal Current (NCC). Red arrows indicate the Norwegian Atlantic Current (NwAC). Blue arrows indicate the East Greenland Current (EGC). The circular black arrows indicate the Lofoten Vortex (LV). The two-headed black arrow indicates Moskstraumen.

135 The LoVe archipelago along northern Norway's coast in Fig. 1 is chosen for this study due to its ecological significance. Complex bottom topography and a steep continental slope steer the region's primary surface currents (Sundby, 1984); the Norwegian Atlantic Slope Current (NwASC) (Rossby et al., 2009) and the Norwegian Coastal Current (NCC) (Gascard et al., 2004) - The fractal coastline and Vestfjorden have large implications on the NCC, causing complex flow features. During winter,

southerly winds cause water mass accumulation along the coast and the geostrophic adjustment to the sea surface tilt can lead to increased current velocities (Mitchelson-Jacob and Sundby, 2001).

140 This particular region where NwASC and NCC converge is a hotspot for intense eddy formation and heat exchange along the Norwegian coast. An unstable front frequently forms between these currents at the steepest continental slope section, caused by lateral and vertical current shear and

The NwASC and NCC meet right off the Lofoten archipelago. The steep continental slope, combined with a narrow shelf, sets up steep fronts that host a range of flow instabilities. The result is the most intense mesoscale eddy field in all of the Nordic Seas and vigorous exchanges of heat, salt and nutrients between the shelf and deep ocean. (Koszalka et al., 2013; Isachsen, 2015; Trodahl and Isaachsen, 2018). As such, the steep slope (Koszalka et al., 2013; Isachsen, 2015; Trodahl and Isachsen, 2018). Eddies formed in NwASC tend to break off and drift westwards, merging with the Lofoten Vortex (Søiland and Rossby, 2013). This region offers a particular challenge with respect to accurate modeling of currents and transport.

2.2 Regional Ocean Ensemble Prediction System

As an example for ocean circulation in a coastal area with temporal varying flow, we use We use flow data from Barents-2.5 EPS (Röhrs et al., 2023), a coupled numerical ocean and sea-ice model an ensemble prediction system based on the regional ocean modeling system (ROMS) (Shepetchkin and McWilliams, 2005) Regional Ocean Modeling System (ROMS; Shepetchkin and McWilliams, 2005). The model has a 2.5 km horizontal grid size and hourly temporal resolution, covering the Barents Sea, the coast off northern Norway and Svalbard (see Fig. 1). The system-EPS consists of 24 members, divided into four sets of six members. The sets are initiated with a 6-hour delay, at 00 UTC, 06 UTC, 12 UTC, and 18 UTC, with a forecast period of 66 hours. Each member is initialized by its own state from the previous day in order to preserve sufficient spread in the ensemble. The EPS forecast is initialized with largely varying perturbed initial conditions in the mesoscale circulation, as to represent model uncertainties. The ensemble spread is further controlled by the Ensemble Kalman Filter data assimilation scheme, which reduces controls the spread of observed variables (Evensen, 1994; Röhrs et al., 2023). The first member in each set (four members) is forced by the most recent atmospheric conditions from the AROME-Arctic model (Müller et al., 2017). The remaining members are forced by 20 members drawn from the integrated forecast system developed by the European Centre for Medium Range Weather Forecasts (ECWF-ENS) (Röhrs et al., 2023).

2.3 Lagrangian Coherent Structures

Various methods have been proposed for LCS detection in 2D flows, among which the FTLE is the most widely used (van Sebille et al., 2018). The distance

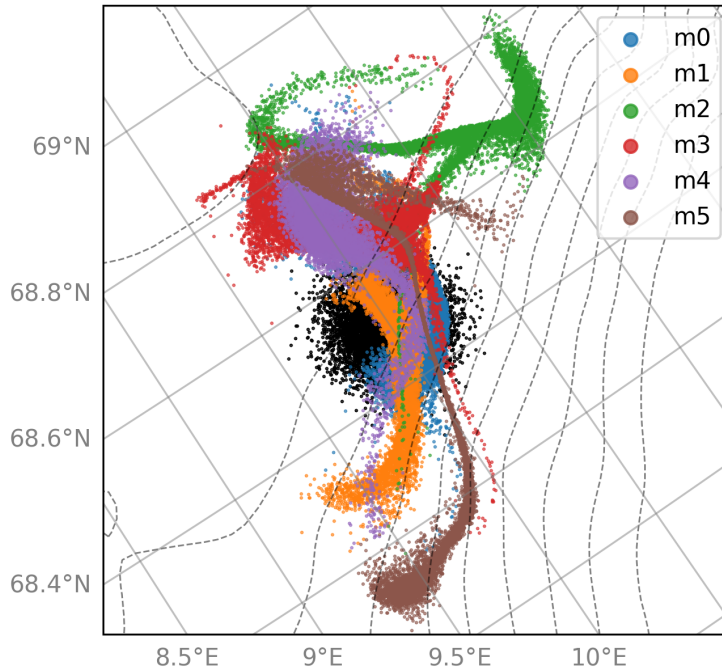


Figure 2. A particle cluster advected for 48 hours from 2023-02-01 using velocity fields from six Barents-2.5 EPS members. Black dots mark the particle clusters initial position.

165 A detailed analysis of particle transport in Barents-2.5 EPS is discussed in de Aguiar et al. (2023), but Figure 2 exemplifies the effect of flow field uncertainty on cluster of particles that have been advected using velocity fields from different ensemble members to showcase. We see that after 48 hours the particle clusters have taken a distinct shape based on the velocity field of the used ensemble member, and an estimated trajectory uncertainty can be obtained from the spread. The trajectory uncertainty is small when flow velocities are similar across the ensemble and increases when there is a large discrepancy between them.

170 2.3 The Finite Time Lyapunov Exponent

A particle will be advected in the presence of an underlying flow field. The trajectory may be obtained by integrating along the encountered flow field:

$$\underbrace{x(t)}_{\text{trajectory}} = \underbrace{x_0}_{\text{initial position}} + \int_{t_0}^t \mathbf{u}(x(\tau)) d\tau. \quad (1)$$

175 Here, $x(t)$ is the position of a particle at time t advected from its initial position x_0 using the velocity field \mathbf{u} along the evolving trajectory locations $x(\tau)$. In this study, particle trajectories are calculated by OpenDrift (Dagestad et al., 2018a), an open-source Python based software for Lagrangian particle modelling developed at the Norwegian Meteorological Institute.

The Lyapunov exponent describes the separation rate between two neighbouring particles in a chaotic system. This separation is assumed to grow exponentially over time in a chaotic system. Therefore, so that the distance δ_t between the two particles at time t can be approximated as a function of the initial distance δ_0 : becomes

$$180 \quad \delta_t \approx \delta_0 e^{\sigma t}, \quad (2)$$

where δ_0 is the initial separation and σ is the Lyapunov exponent, i.e. the separation rate (Rosenstein et al., 1993). FTLE finds the maximum separation rate between infinitesimal fluid parcels over a finite time interval (Pierrehumbert and Yang, 1993). Because FTLE measures separation, i.e. repulsion, Haller (2001) and Shadden et al. (2005) argue that FTLE can identify repelling hyperbolic LCSs.

185 The LCS theory originates from the Lagrangian viewpoint, aiming to examine fluid transport based on Lagrangian principles. The FTLE method calculates the separation rate among fluid elements at fixed model grid points. Consequently, despite its Lagrangian roots, the FTLE information is on an Eulerian grid. over a finite time interval (Pierrehumbert and Yang, 1993).

FTLE's are calculated from flow fields provided by an OGCM following the method described by Haller (2001); Shadden et al. (2005); F. Haller (2001), Shadden et al. (2005) and Farazmand and Haller (2012). The 2D movement of fluid parcels from their initial positions $\mathbf{x}_0, \mathbf{x}_0 = (x_0, y_0)$ at time t_0 to their final positions at time t is described by a flow map $\mathbf{F}_{t_0}^t(\mathbf{x}_0)$. As multiple fluid parcels are transported by the flow, the distance between neighbouring fluid parcels is likely to contract or expand over the time interval. At each point in space, the change in separation between fluid parcels can be described by the Jacobian of $\mathbf{F}_{t_0}^t(\mathbf{x}_0)$:

$$190 \quad \nabla \mathbf{F}_{t_0}^t(\mathbf{x}_0) = \begin{bmatrix} \frac{\partial x}{\partial x_0} & \frac{\partial x}{\partial y_0} \\ \frac{\partial y}{\partial x_0} & \frac{\partial y}{\partial y_0} \end{bmatrix}, \quad (3)$$

195 where $\partial x_0, \partial y_0, \partial x,$ and ∂y are the initial and final distances between particles in x and y directions. ∂x and ∂y are obtained by advecting fluid parcels:-

$$\underline{\partial x = \int \mathbf{u} \delta t},$$

where $\mathbf{x} = (x, y)$ is the parcels' position and $\mathbf{u} = (u, v)$ (x, y) is the velocity field. This advection is calculated by OpenDrift (Dagestad et al., 2018b), an open-source Python-based software for Lagrangian particle modelling developed at the Norwegian Meteorological Institute final position of a fluid parcel which was initially located at (x_0, y_0) . These positions may be obtained from Eq. 1. The matrix entries in Eq. 3 are the partial derivatives of the final position relative to their initial position. Eq. 3 is used to define the Cauchy-Green strain tensor $\mathbf{C}_{t_0}^t(\mathbf{x}_0)$ (Truesdell and Noll, 2004), which describes the speed and direction of deformation in the system

$$200 \quad \mathbf{C}_{t_0}^t(\mathbf{x}_0) = [\nabla \mathbf{F}_{t_0}^t(\mathbf{x}_0)]^* \nabla \mathbf{F}_{t_0}^t(\mathbf{x}_0). \quad (4)$$

205 It can then be shown that the FTLE field is given by the FTLE is then defined using $\mathbf{C}_{t_0}^t$:

$$\sigma_{t_0}^t(\mathbf{x}) = \frac{1}{|T|} \ln \sqrt{\lambda_{max}(\mathbf{C}_{t_0}^t)}, \quad (5)$$

where T is the time interval, chosen as 24 hours for our simulations, over which the FTLE is computed and $\lambda_{max}(C_{t_0}^t)$ is the largest eigenvalue of $C_{t_0}^t(x_0)$ corresponding to the dominant stretching direction (eigenvector) in the system. It can be shown that repulsion in a system is attraction in the same system over a reversed time-frame. Thus, a repelling LCS over the backwards time interval is an attracting LCS over the forwards time interval. The absolute value of T allows for integration both forwards and backwards in time. Finding the largest FTLE (largest stretching) If one uses FTLE as an LCS detection tool, a forward-in-time will result in detection of repelling LCSs, whereas the largest FTLE computation will correspond to repelling LCS, whereas a backward-in-time yield attracting LCSs forward-in-time (Haller, 2001; Shadden et al., 2005; Farazmand and Haller, 2012). Attracting LCSs are interesting from an ecological standpoint, as these can e.g. describe nutrient or pollution accumulation regions. We will therefore focus on attracting LCSs, although LCS robustness and persistence should apply for both. computation will correspond to attracting LCS (Haller, 2001; Shadden et al., 2005; Farazmand and Haller, 2012).

In this study we will investigate FTLE computed from backward-in time integrations. Furthermore, the study is motivated by typical uses of ocean forecasting models, which are decision support tools for search-and-rescue operations, oil-spill and ice-berg forecasts and similar trajectory analyses. These often operate at time-scales from a few hours up to a few days, and therefore, we will predominantly use $T = 24$ hours for the FTLE computations. But we also provide some discussion of the choice of T in Sec. 3.1

FTLE averages over ensemble members and time are calculated to identify robust and persistent features. Variations among members and over time are expected due to perturbed velocity fields and time dependency. Averaging might unveil similarities across both members and time. The notations \bar{F}_m and \bar{F}_τ denote over time periods will be calculated to characterize robustness and persistence, respectively. For each such analysis, we first compute the FTLE fields from a set of flow fields and thereafter calculate averages over those FTLE fields, which is similar to the D-FTLE mean method discussed in Guo et al. (2016). We define the ensemble and time averages, respectively. The standard deviation gives a measure of the spread in the sample distribution, and is denoted as σ_m as:

$$\bar{F}_m = \frac{1}{N} \sum \sigma_{t_0}^t(m) \quad (6)$$

$$\bar{F}_\tau = \frac{1}{N} \sum \sigma_{t_0}^t(\tau), \quad (7)$$

where $\sigma_{t_0}^t(m)$ and σ_τ for the ensemble and time standard deviations, respectively $\sigma_{t_0}^t(\tau)$ are the FTLE fields over the given time interval for ensemble member m or over a specific time-period τ , and where N is the total number of fields being averaged. So, for example, for time interval $T = 24$ hours, τ will indicate the specific daily FTLE field from a set of multiple daily fields.

LCSs, which are infinitesimally thin 1D curves in 2D flow fields are approximated by FTLEs with 2D curves with a finite width. A conceptual example of FTLE ridges and their average is shown in Fig. 2. The ridges act as repellers or attractors at distinct locations. Averaging smooths the ridges into a field of repulsion/attraction. Variations among ensemble members and over time are expected due to perturbed and time-evolving velocity fields. It is thus expected that averaging FTLE fields will smooth out non-robust and non-persistent features while highlighting robust and persistent features, ultimately indicating a region where FTLE ridges regions where high FTLE values are statistically likely to form. On the other hand, if the individual

240 FTLE ridges would be more similar to each other, linear features should still be present in the average, making these ridges more certain and/over ensemble members or frequently form over time. Certain features or 'ridges' in the averaged FTLE fields may also be discerned, in which case these should be considered highly robust or persistent. These regions are strong potential candidates for robust or persistent material accumulation regions.

245 The ensemble average, \overline{F}_m , and the time average, \overline{F}_t , should not be considered as definitive transport barriers. It is unclear whether LCSs constituting these averages originate from the same model realization or exist simultaneously. It is also uncertain whether an average consists of a few long LCSs or many short ones. The former act as transport barriers over larger regions, while the latter permit material drift between them. We note that a time-average or ensemble average description of FTLE could also be performed by first averaging the flow field, and then calculating the FTLE. This procedure has the caveat that the flow maps used in Eqns. 2 and 3 is not based on time-evolving flow fields, and hence do not identify realistic deformation and accumulation. Instead, we consider \overline{F}_m and \overline{F}_t as average accumulation or dispersion regions, potentially containing transport barriers aim for a statistical description of flow features by analysing the mean and spatial structure of realistic FTLE fields.

3 Results

255 Firstly, we present the temporal evolution of the Below, we first have a quick look at how the choice of integration time impacts the FTLE field, assessing this in relation to applications relevant for operational oceanography. We then look at whether there is in fact any persistence or robustness in FTLE and detect persistent FTLEs through the time average. Secondly, FTLEs from individual EPS members and their average are presented to highlight uncertainties in the FTLE field given an uncertain velocity field to detect robust features fields over the dynamically active LoVe region. Finally, spatial and we do a spectral analysis of the FTLE fields are presented to provide a more comprehensive analysis of FTLE robustness and persistence field in an attempt at pin-pointing the resolution needed for practical use in an operational forecasting system.

260 3.1 Persistence of Lagrangian Coherent Structures Integration time

Instantaneous surface velocity fields (top row) and corresponding FTLE ridges that approximate attracting LCSs (bottom row) during four selected dates: a,e) 2023-02-01, b,f) 2023-02-08, c,g) 2023-02-14, and d,h) 2023-02-21 at time 00:00. The bathymetry is indicated by gray dashed lines. Two persistent eddies are highlighted with blue boxes. Velocity fields and corresponding backwards FTLEs from first AROME-Arctic-driven member (henceforth called the reference member) of the Barents-2.5 EPS- Backwards-in-time FTLE fields, all starting from the same t_0 at 2021-12-31 but using different integration lengths T , are shown in Fig. 3 for four exemplary dates one week apart in February 2023. Note that FTLE ridges approximate LCSs. Additional criteria for a distinction of LCS from FTLE fields are given by Farazmand and Haller (2012) but are not evaluated here. Hence, we evaluate the variability of FTLE fields:

270 The intensity and meandering of the coastal current, as well as details in the eddy field change from week to week in Figs. 3a-d. However, Figure 1. The values are normalized as the FTLE values tend to decrease with increasing T . As noted by e.g. Wilde et al. (2018) and Peng and Dabiri (2008), a longer integration time tends to result in sharper FTLE ridges. We note,

however, that the overall structure of the FTLE field is not overly sensitive to the two highlighted eddies are present in the three first weeks. These are considered to be persistent flow features over the time period.

275 The FTLE field changes in Figs. 3e-h along with the velocity field. In general, no FTLE ridges stay the same between the time steps, even in regions where the flow itself appears largely persistent, e.g. the two highlighted eddies. Thus, the associated LCS are highly ephemeral, changing rapidly with the flow.

280 We note that there are more FTLE ridges in the domain in the first time step, indicating that velocity gradients cause material accumulation. This can e.g. be seen in the eddies in the region, which are often represented by circular linear features in integration period within the integration length of 12 to 72 hours, although the features in the field are more detailed for the 72-hour period than for 12 hours. For even longer integration periods there is clear indication that distinct FTLE features in the energetic flow regions over the continental shelf and slope are smeared out. A plausible interpretation is that the ability of the FTLE field to describe flow field features depends on the integration period that matches the time scale of the dynamics. This advective time, which scales as L/U (for velocity scale U and length scale L), then depends on environmental conditions. So capturing highly energetic small-scale features associated with the fronts over the continental shelf and slope require short integration times. In contrast, low-energy and large-scale features over the deep basin are slow enough to be well-represented by FTLE integrations that have been conducted over several days.

285 We know that even though the flow field is changing, some flow features will always exist on average over time. In the case of the LoVe region, strong currents along the continental slope (NwAC and NCC) are present on average. Similarly, FTLEs vary in time, but certain regions frequently exhibit FTLE ridges. The FTLE time average, \overline{F}_t , will reveal these regions. The FTLE time average, \overline{F}_t , will reveal these regions to describe flow field features depends on the integration period that matches the time scale of the dynamics. This advective time, which scales as L/U (for velocity scale U and length scale L), then depends on environmental conditions. So capturing highly energetic small-scale features associated with the fronts over the continental shelf and slope require short integration times. In contrast, low-energy and large-scale features over the deep basin are slow enough to be well-represented by FTLE integrations that have been conducted over several days.

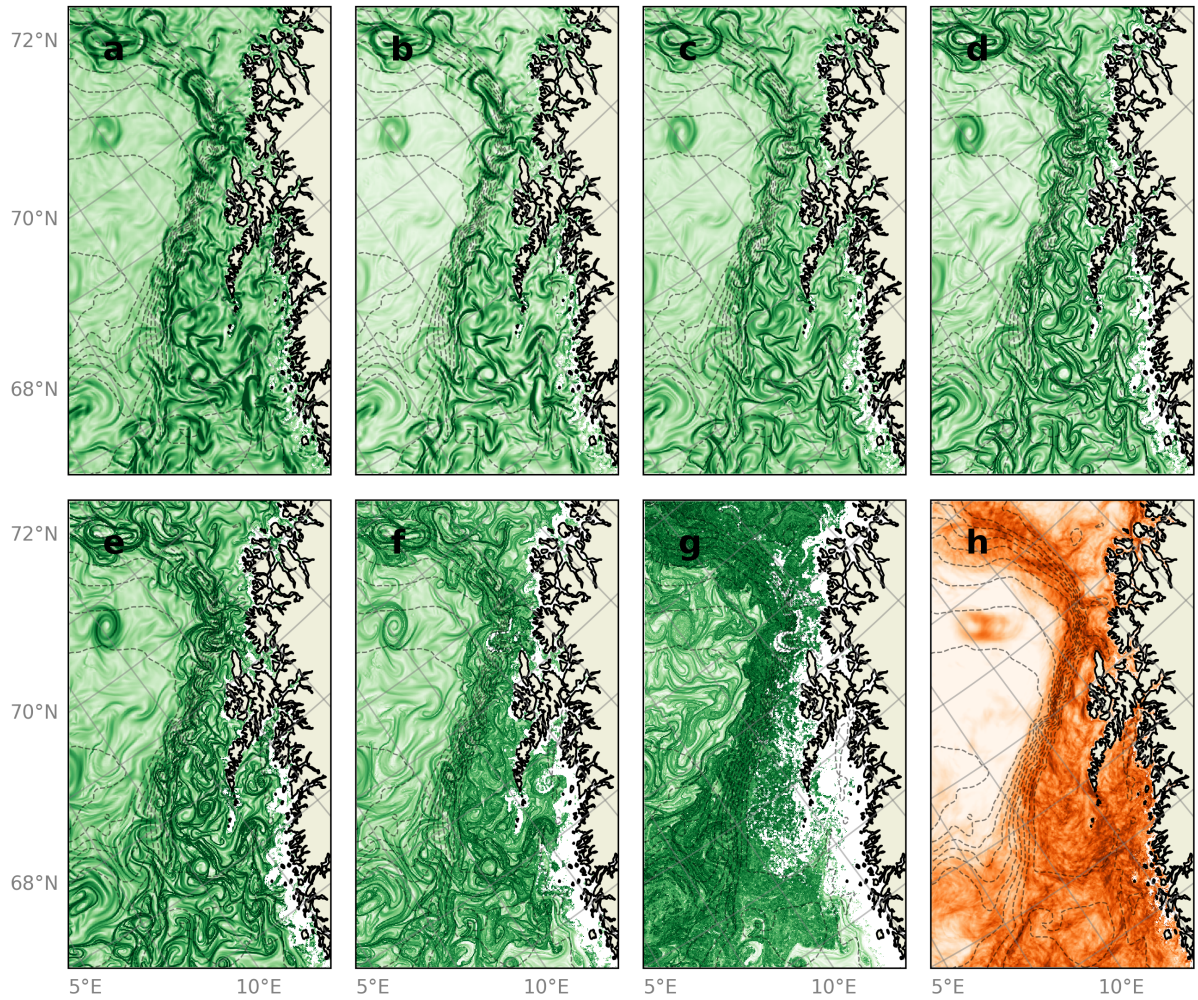


Figure 3. Normalized FTLE time averages, \bar{F}_T , (orange) and standard deviation over time, σ_T (blue) around the LoVe region for four computed for different time periods values of T , all starting on 2023-02-01: at 2021-12-31. a,e) 7 days 6 hours, b,f) 14 days 12 hours, c) 24 hours, g,d) 21-48 hours, e) 72 hours, f) 168 hours (7 days) and d,h) 672 hours (28 days). The FTLE analysis is based on velocities from a single ensemble member (reference member h) monthly average of the Barents-2.5 EPS FTLE fields computed with $T = 24$ hours. Dashed Bathymetry indicated with gray dashed lines indicate bathymetry.

295 FTLE averages and standard deviations over time, \bar{F}_T and σ_T , are shown in Fig. 4 for different averaging lengths. Longer averaging periods effectively reduce variability in \bar{F}_T . Strong linear features in \bar{F}_T can be distinguished for shorter averaging times in the domain, indicating a degree of short-term persistence. However, these features become more diffused in \bar{F}_T with higher averaging periods, and individual FTLE ridges disappear for averaging times of 30 days or longer.

Even though FTLE ridges are seen to be ephemeral in Fig. 3, high-valued \bar{F}_T regions indicate where FTLE ridges are frequently situated over time. Most notably, \bar{F}_T indicates frequent FTLE ridges along A time-averaged FTLE field is also shown

in Figure 3h. This is included to illustrate that the FTLE analysis based on long integration periods (e.g. over 168 and 672 hours) are distinctly different from the time-averaged FTLE field of several 24-hour integration periods. The time-averaged FTLE field should be interpreted as highlighting regions that are *typically* abundant with high FTLE values over the time period. The calculation reveals that in this particular region, structures forming high FTLE values are most often found over the continental slope during February 2023, where the mean flow is most significant. FTLE ridges are less frequent on the continental shelf and . In contrast, the FTLE structures appearing over the deep ocean. Both notions are independent of averaging time. Furthermore, the two eddies indicated in Fig. 3 are persistent in the mean flow in Fig. 1, and frequent FTLE activity is present in the same regions. This result indicates that, unsurprisingly, FTLE ridges are persistent where the current itself is persistent. basin when FTLEs are calculated over long integration periods wash out in the average description.

~~The large variability over time~~

3.2 Persistence over time

Velocity magnitude fields and corresponding backwards FTLE fields from the first member of the Barents-2.5 EPS (henceforth called the reference member) are shown in Figure 3 for three example dates one week apart in January 2023, along with the monthly-averaged velocity and FTLE fields. As expected, the continental slope current is further emphasized by the standard deviation σ_t . Regions with high \bar{F}_t are usually accompanied by high σ_t , affirming a positional and structural evolution. Note that σ_t will be large with small positional perturbations of FTLE ridges shown to be persistent over the time period. But the intensity and meandering of the current change from week to week, and this time variability projects onto the FTLE fields as few features there stay the same between time steps. And yet, there is clearly a concentration of high-magnitude FTLE features over the steep continental slope during this time period—as effectively summarized by the time-averaged FTLE field, \bar{F}_t . The interpretation is that strong FTLE features are expected to be frequent along the continental slope, at least over this sample time period, even though the FTLE average over time does not yield detailed information about how these look like as individual features.

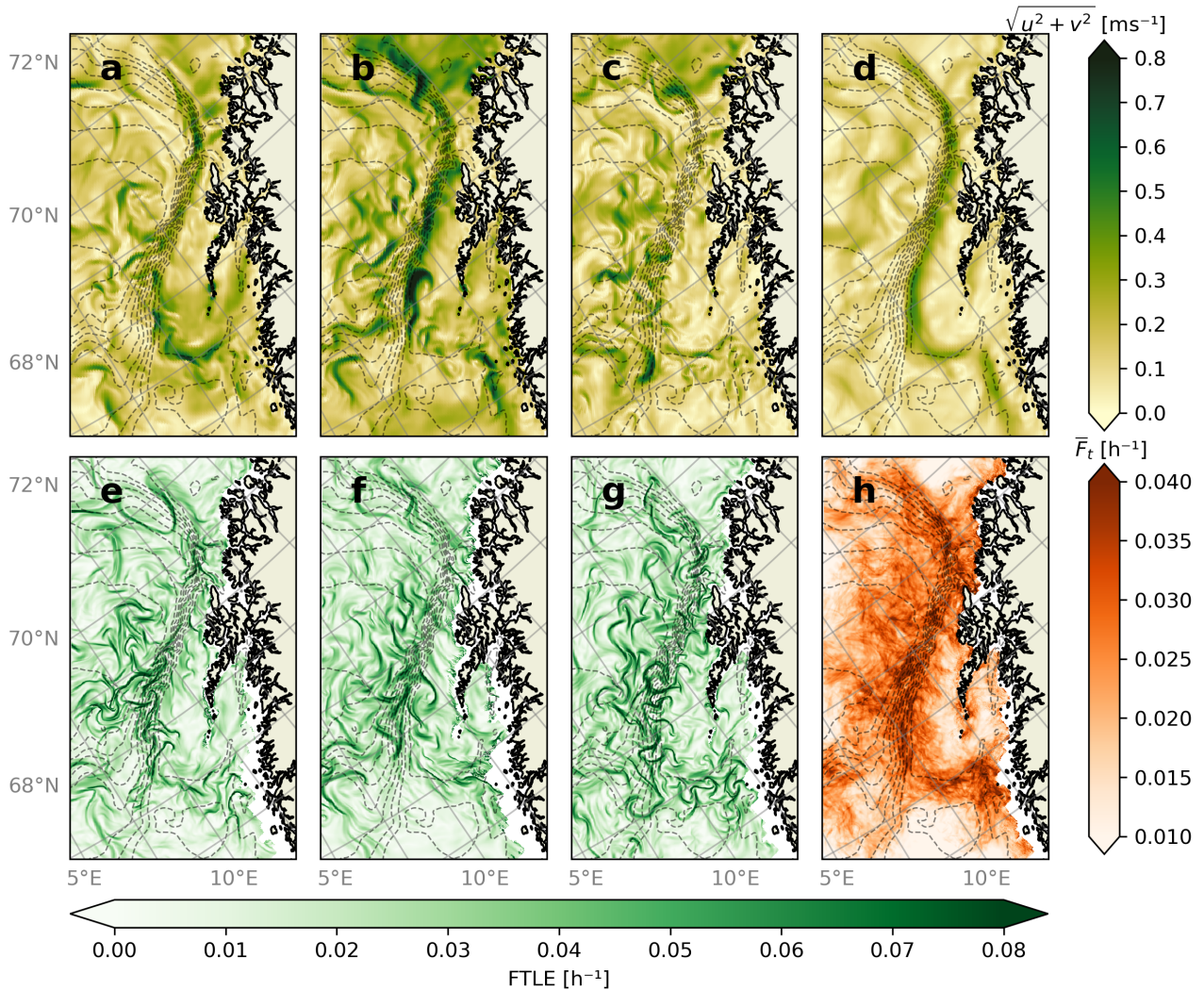


Figure 4. Seasonal FTLE averages for instantaneous velocity fields (top row) from the reference member of Barents-2.5 EPS at a) winter and 2023-01-02, b) summer. Months included in the winter season are December 2022, January 2023, 2023-01-08 and February-c) 2023-01-15 at 00:00, d) averaged velocity field for January 2023. Months included in summer season are June 2023, July 2023, Backwards FTLE fields (bottom row) computed with $T = 24$ hours over e) 2023-01-02 f) 2023-01-08 and August-c) 2023-01-15, h) monthly average of daily FTLE fields for January 2023. Dashed gray lines indicate bathymetry.

Seasonal

To highlight the permanent impact of the continental slope, seasonally-averaged velocity fields are shown in Figure 4 along with seasonal FTLE averages, \bar{F}_t , for the winter and summer seasons are shown in Fig. 5. FTLEs indicate a frequently occurring

325 transport barrier computed from daily FTLE fields from the summer and winter seasons. The slope current is placed similarly in
 both seasons, although it is stronger during winter, likely due to a geostrophic adjustment to the sea surface tilt, as discussed in
 Sec. 2.1. On the other hand, \overline{F}_t changes drastically between the two seasons. We see that strong values in the FTLE field along
 the continental slope during winter, but not during the summer season. Both seasons exhibit large activity near the northern tip
of LoVe, with the summer season showing higher activity around Moskstraumen occur much more frequently during winter.
 Large values can be seen for both seasons near the coastline, which are suspected to be produced by strong horizontal velocity
 330 shear near the coastal regions.

The high \overline{F}_m around Moskstraumen

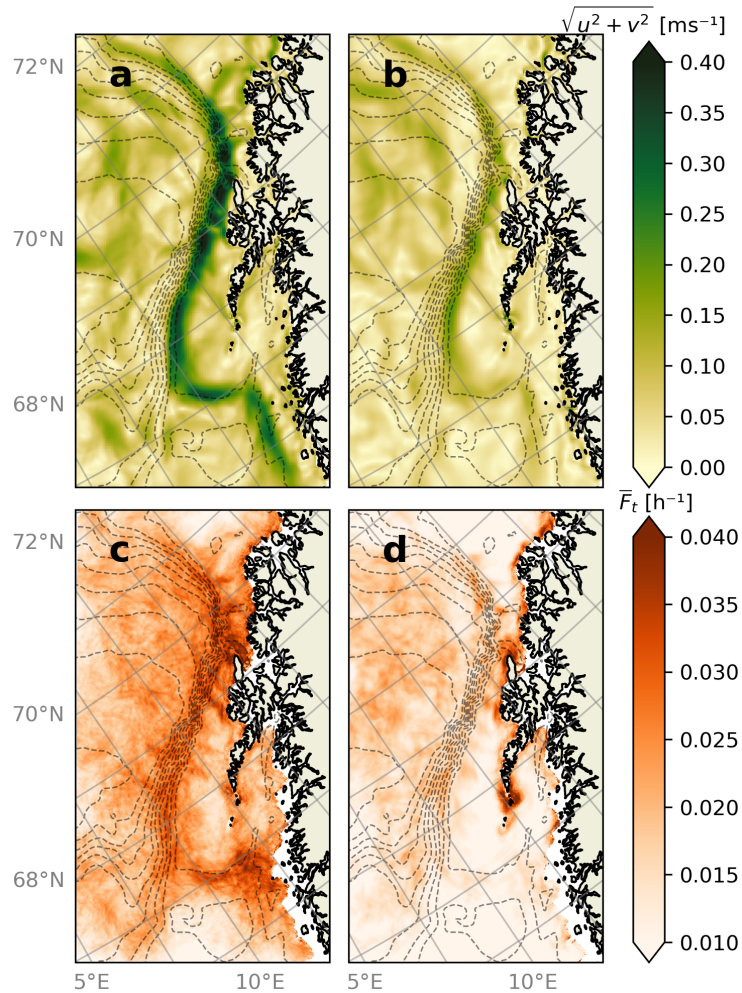


Figure 5. Seasonal FTLE averages for a) winter and b) summer. Months included in the winter season are December 2022, January 2023, and February 2023. Months included in summer season are June 2023, July 2023, and August 2023. Dashed gray lines indicate bathymetry.

335 Near the coast, a region of high \overline{F}_t around Moskstraumen strait (at the southern tip of the LoVe archipelago; see Fig. 1), especially during summer, is directly connected to the formation of strong jets at the strait exit. The direction of the current through the strait is dependent on the tidal phase (Børve et al., 2021). After closer investigation, FTLE ridges using $T = 2$ hours for the FTLE time interval, high values in the FTLE field tend to form only on one side of Moskstraumen at any particular time, depending on the current direction and thus the tidal phase. Therefore, a predictable tidal-dependent periodic variability of FTLEs exists here. An indication of this phenomena is seen to a lesser extent during winter may exist here. FTLE has previously been shown to be highly sensitive to the tidal phase (Zhong et al., 2022). However, the models spatial resolution may be too low to fully resolve the currents in this region, and a closer investigation into the dynamics at play here will need to be left for a future high-resolution model study.

3.3 Robustness of Lagrangian Coherent Structures (a,b,c,d) Velocity fields from four different Barents-2.5 EPS ensemble members at the LoVe region at 2023-02-01 and e,f,g,h) corresponding backward FTLEs. Two regions of interest are highlighted with blue boxes. We investigate the over ensemble realizations

345 We turn next to the concept of robustness of FTLE predictions, i.e. whether FTLE ridges predicted by an OGCMs are similarly present in an ensemble of flow realisations. Velocity fields and FTLEs of four fields, that is the extent to which FTLE fields computed using flow fields from different EPS realizations are similar. As an example, velocity fields and FTLE fields of three randomly selected members are shown in Fig. 6. Generally, the displayed set of FTLE fields show that FTLE ridges appear in similar regions, but their position is shifted and linear features have different lengths and shapes. Nevertheless, we identify particular FTLE ridges that exist across ensemble members, with slight variations.

350 Two regions containing eddies in the flow field are highlighted with boxes in Fig. 6. The eddies in the highlighted regions are generally represented by circular FTLE ridges. A clearly defined eddy is found in box A in all members, with member 1 containing two eddies. The bottom eddy in member 1 has a similar position to the eddy in member 0, whereas the top eddy in member 1 has a similar position to the eddies in members 2 and 3. The eddies in box A in members 1-3 are represented by clearly defined circular FTLE ridges. Ignoring the bottom eddy in member 1, these circular FTLEs center around approximately the same point, although the shape and sizes of the circles vary. However, it is hard to discern the eddy in member 0 in the FTLE field, even though it appears to be similar to the bottom eddy in member 1. Box B highlights another eddy which is similar between members, both in position and size. The FTLE representation appears similar, although the circle in member 0 appears rougher than in the rest.

360 On closer inspection, all members of the Barents-2.5 EPS predict eddies in the box A region, some of which predict one eddy in a similar position to members 2 and 3 in Fig. 6, whereas others predict two or more eddies, similarly to member 1. However, some members represent the eddies with circular FTLE ridges, whereas the circles are hard to discern in other members. A similar analysis of the region in box 2 reveals that this eddy is present in most members, hence is considered to be certain. Differences in FTLE ridges are more apparent than in the flow field Figure 6, and similar flow features can have both similar or different FTLE representations along with the ensemble-averaged velocity and FTLE field. We see that the individual ensemble members all contain a strong current along the continental slope, which has also been shown to be a time-persistent current.

370 However, and as expected from a highly nonlinear and chaotic flow field, the position and strength of individual eddies and current meanders vary considerably between members. This is certainly the case for small-scale structures along the slope current. But some larger-scale mesoscale structures over the deep ocean, e.g. a vortex in the south-western corner of the domain, are actually predicted by all three ensemble members. Such large-scale features thus survive the smoothing inherent in the ensemble-averaged velocity field, whereas most individual small-scale structures are washed out. Plainly speaking, the EPS gives a low confidence that any of these small-scale structures actually exist in the real ocean at their specific location at this particular time.

FTLE fields around the LoVe region at 2023-01-02 (top) and 2023-02-02 (bottom) computed using velocity fields from the Barents-2.5 EPS. a,d) FTLE fields (green) from member 0. b,e) averaged FTLE fields (red) over the ensemble. c,f) standard deviation of the FTLE fields (purple) over the ensemble. Bottom topography indicated with dashed gray lines:

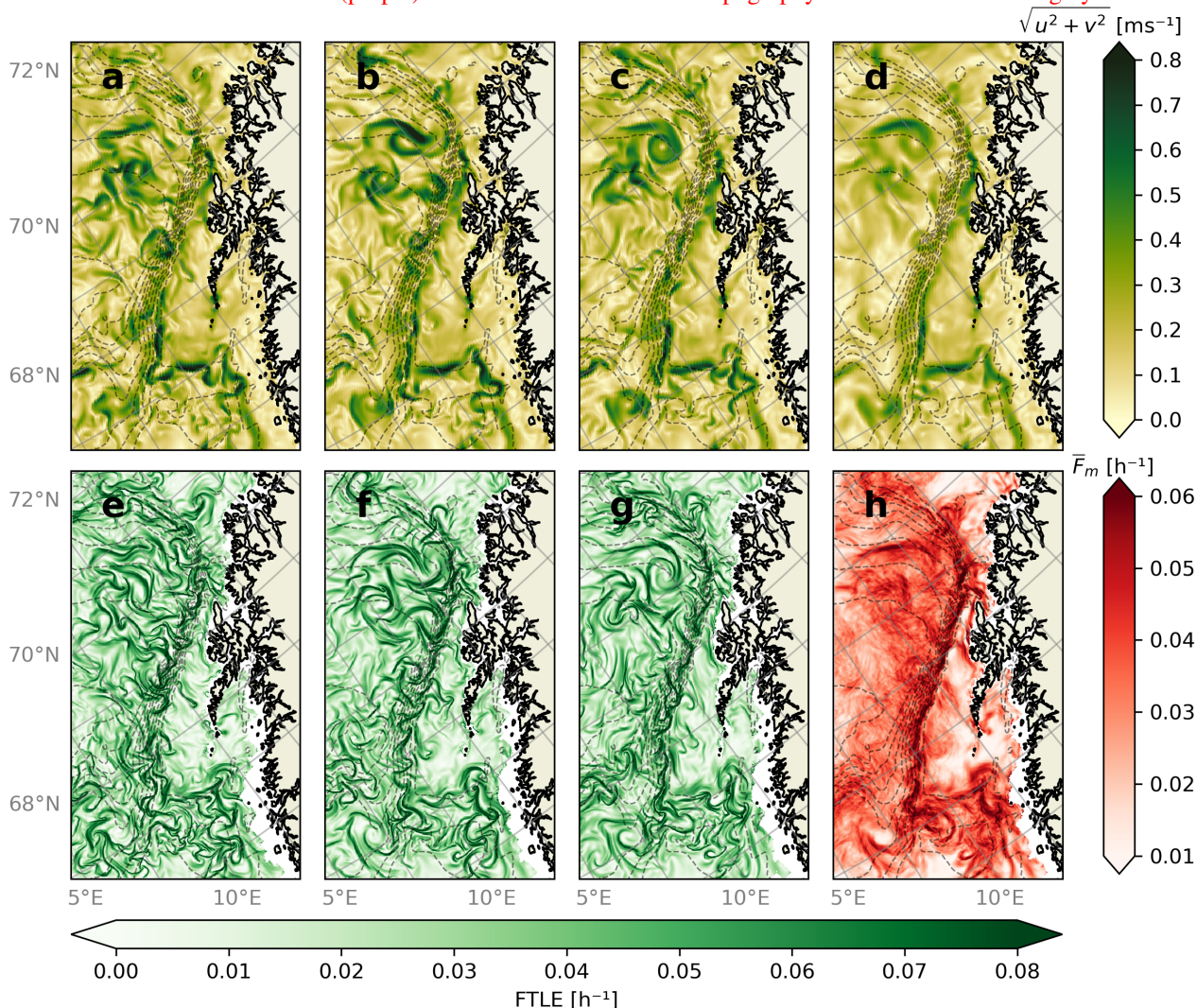


Figure 6. a, b and c) Velocity fields from three different Barents-2.5 EPS ensemble members at the LoVe region at 2023-02-02 00:00 and d) ensemble averaged velocity field over all EPS members. e, f and g) backwards FTLE fields computed over 2023-02-01 for the members shown in a, b and c. h) The ensemble averaged FTLE field.

~~Instead-~~

375 The flow variability within the ensemble again projects directly onto the FTLE values, and, as expected, there is generally little one-to-one agreement between the three ensemble members displayed here. But we see that all the members of the ensemble predict high FTLE values along the continental slope, as well as in the eddy-dominated deep basin region at 70.5°

latitude. But the exact positions and strength of FTLE maxima vary considerably and even more so than the velocity field itself. Again, we must interpret this as indication that the FTLE field from one single model integration may not reflect conditions in the real ocean at any specific time.

380 Thus, instead of inspecting the FTLEs FTLE fields of each member individually, ~~the ensemble-averaged a study of the ensemble-averaged~~ FTLE field, \bar{F}_m , allows us to detect robust features; ~~linear features flow features; high values~~ will be present in \bar{F}_m where ~~multiple (but not necessarily all)~~ individual members predict ~~the FTLE ridges similarly. FTLE fields for the reference member, \bar{F}_m and the ensemble standard deviation FTLE, σ_m , are shown for two dates in Fig. 7. Both dates exhibit clearly distinguishable linear features in \bar{F}_m along the continental slope, although these are stronger and longer on 2023-02-02.~~
385 ~~While these linear features in high FTLE activity. In the situation studied here, \bar{F}_m are long, continuous and shows a long and continuous feature~~ tangent to the continental slope, ~~FTLE ridges. However,~~ in individual members ~~are thinner, shorter the features formed by high FTLE values are seen to be disjointed, thinner~~ and often not tangent to the continental slope. \bar{F}_m shows where majority of members predict FTLE ridges, but not exactly how these look like. A large σ_m further emphasizes the structural and positional variability of individual FTLE ridges along the continental slope. Even so, because of the strong
390 signal in \bar{F}_m , the FTLEs along the continental slope are robust.

Two additional regions are identified and considered as robust in Fig. 7. These are the u-shaped structure in the north at 2023-01-02 and the circular shape in the south at 2023-02-02, which are enlarged in Fig. 8. The u-shaped structure exhibits thin, distinguishable features with little noise around them, and corresponding σ_m indicates small variability around \bar{F}_m , implying high agreement between members. Inspecting each member individually reveals this to be true, thus linear features
395 in \bar{F}_m represent individual members well. This u-shaped structure is therefore highly robust at this particular time.

Detailed map of the two regions highlighted in Fig. 7. a) ensemble average for 2023-01-02, b) ensemble standard deviation for 2023-01-02, c) ensemble average for 2023-02-02, and d) ensemble standard deviation for 2023-02-02. The circular-linear features in \bar{F}_m in Fig. 8 represent the same eddy as seen in Fig. 7 one day later. There is more noise around this feature than the u-shaped structure, but a circle can still be distinguished in \bar{F}_m . Individual members generally agree on this feature, but
400 disagree on the FTLE field around said structure. The large σ_m reveals that members disagree on its exact shape and position. Therefore, this structure can be considered robust, although its exact appearance is more uncertain than the u-shaped structure.

Finally, there is a region to the left of ~~The eddy-dominated region at 70.5° latitude also contains high averaged FTLE values, but these are smoother than over~~ the continental slope in Fig. 7b which exhibits high values in \bar{F}_m , but all linear features
405 have been smoothed out. Combined with the high σ_m in this location, it can be concluded that there is a high probability of strong linear features existing in this region, but these are non-robust and their position and shape is indeterminable from \bar{F}_m . Therefore, an FTLE average can, ~~thus presumably reflecting typical occurrences of strong FTLE features but also a lower impact of bottom bathymetry. An FTLE average may thus~~ yield both distinguishable linear features in the domain, ~~which can be considered as robust features,~~ as well as large smooth fields. ~~Linear features are associated with robustness, indicating~~
410 higher certainty, whereas a smooth field yields regions where linear of higher FTLE values, which indicate that strong features are likely to be found. Often a high \bar{F}_m is accompanied by a high σ_m , but this might simply be a result of small positional

perturbations of the thin linear curves, and does not necessarily indicate significant variability. Therefore, the highlighted regions are considered to be robust for the particular dates here but are more variable across the ensemble.

3.4 Properties of ensemble and time averaged FTLE fields

415 Spatial and spectral variance of FTLEs and averaged FTLEs. a) Spatial variance over the ensemble average. Thin blue and red graphs indicate individual days during the winter and summer seasons, and the thicker blue and red graphs are the average of the thin graphs. b) Spatial variance over the time average. Thin purple and green graphs indicate the evolution of variance during the winter and summer months as up to 30 days are considered in the time average for each member. c) Spectral distribution of spatial FTLE variance in ensemble averages as an increasing number of members are considered in the average, averaged
420 over all days in winter. d) Spectral distribution of spatial FTLE variance for time averages as an increasing number of days are considered in the average, starting from 2023-01-01, averaged over all members. Colorbars in c) and d) indicate how many members or days the FTLE fields are averaged over. We wish to investigate how the energy distribution of FTLEs over different spatial scales change when averaged over the ensemble or time. One method for conducting the spectral analysis on 2D fields is the discrete cosine transform (DCT) proposed by Denis et al. (2002).

425 Robustness and persistence of FTLEs are compared by their spatial and spectral variance, shown in Fig. ???. The spatial variance has been computed by averaging FTLEs over an increasing number of members or days, then computing the variance over the resulting averaged FTLE field. For the spectral variance, We select three 200km×200km non-overlapping sections without land have been selected. Each section is transformed into Fourier space, and the power spectrum is computed for each grid row and column. Resulting power spectrum over all rows and columns over all sections are then averaged to produce the
430 final spectral variance shown in Fig. ???. Similarly to of the domain away from landmasses. Following Denis et al. (2002), the DCT produces an N_i by N_j field $F(m, n)$ of spectral coefficients, where m and n are adimensional wavenumbers. For a square domain where $N_i = N_j = N$, the wavelength is given by

$$\lambda = \frac{2N\Delta}{k}, \quad (8)$$

where Δ is the grid spacing and $k = \sqrt{m^2 + n^2}$ is a normalized radial wavenumber. To study how the spectral variance of
435 FTLE evolves with time and ensemble averaging, we first compute the average FTLE field over an increasing number of days and members. The results are shown in Figure 7 along with the spatial variance, the FTLE fields are first averaged.

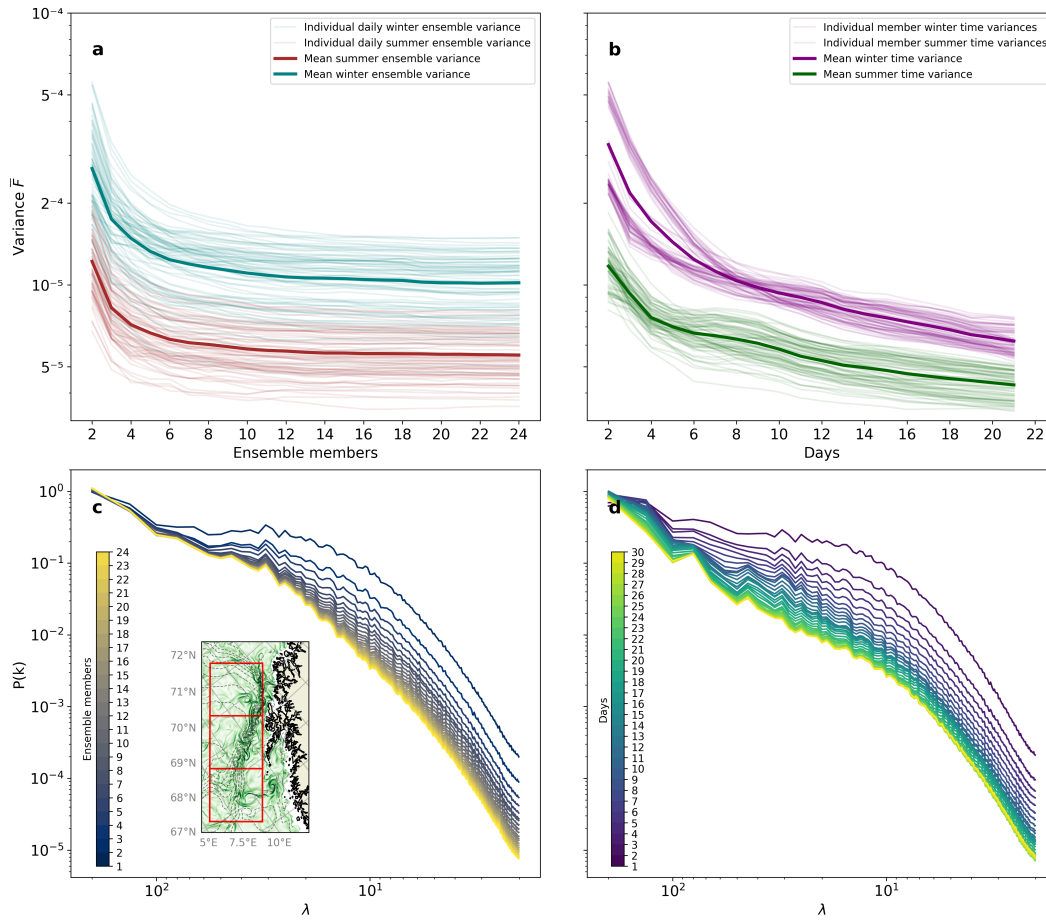


Figure 7. Spatial and spectral variance of FTLEs and averaged FTLEs. a) Spatial variance over the ensemble average. Thin blue and red graphs indicate individual days during the winter and summer seasons, and the thicker blue and red graphs are the average of the thin graphs. b) Spatial variance over the time average. Thin purple and green graphs indicate the evolution of variance during the winter and summer months as up to 21 days are considered in the time average for each member. c) Spectral distribution of spatial FTLE variance in ensemble averages as an increasing number of members are considered in the average, averaged over all days in January 2023. The red squares in the randomly selected FTLE field in c) indicate the regions selected the spectral variance computation. d) Spectral distribution of spatial FTLE variance for time averages as an increasing number of days are considered in the average, starting from 2023-01-01, averaged over all members. Colorbars in c) and d) indicate how many members or days the FTLE fields are averaged over.

The spatial variance has been computed by averaging FTLE fields from the three $200\text{km} \times 200\text{km}$ sections over an increasing number of members or days before conducting this computation of the spectral variance.

The spatial variance ascertains, then computing the variance over the resulting averaged FTLE field. Spatial variance ensures that the degree of smoothing increases as more members or time steps are considered in the FTLE averages. The results suggest that the smoothing rate of FTLE fields is independent of season, although. The value of the variance is lower during summer

due to lower FTLE activity as seen in as FTLE values are generally smaller compared to winter (Fig. 5. This smoothing factor is strong and similar for both averages for the first ~ 5 members and time steps). The strong decay in at the beginning of the \bar{F}_m variance implies that there is a sufficient spread in the ensemble, although. Note that \bar{F}_m is dependent depends on which members are included in the average for few members, which might affect the results as there is a possibility that any randomly selected member might deviate largely from other members. \bar{F}_m becomes less sensitive to a strongly deviating member as more members are included in the average. The spatial variance of \bar{F}_m stabilizes once ~ 10 members are considered, implying the existence of distinct non-chaotic and highly predictable flow features in the ensemble. Meanwhile, the spatial variance of \bar{F}_t continues diminishing, signifying that FTLE ridges fields are more robust over many members than persistent over long time periods.

The spectral variance shows how energy is distributed across wavenumbers over wavelengths. Energy diminishes as more members and time steps and are included in the averages, with the energy dissipation rate being largest for few members and time steps as a result of smoothing of the fields at all wavelengths, coherent with the smoothing factor in the spatial variance. Energy dissipates stronger similarly for smaller wavelengths, and significantly faster for \bar{F}_t than \bar{F}_m at all wavenumbers, but is similar at the largest wavenumbers, i.e. smallest scales. Small scale flows, thus also small scale FTLE ridges, for large to mid wavelengths. Small-scale flows and thus also small-scale FTLE features are generally chaotic and short-lived, thus are and these are therefore uncertain between members and evolve rapidly. Energy dissipates slowest at the largest scales, as large scale flow features are generally less chaotic and more predictable and persistent. Minimal energy dissipation is seen at the largest scales for \bar{F}_m , signifying that large scale structures are generally over time. FTLE features are expected to smooth slower at large scales as flows are less chaotic here. Large-scale structures are more or less certain in the ensemble, whereas they are seen to evolve and drift over time at all scales (albeit slower at the largest wavelengths).

These results show that FTLE ridges. The decay of variance as more FTLE fields are included in an average (Fig. 7a vs. Fig 7b) indicates that FTLE features are more robust than persistent at all scales. Energy dissipation happens fastest at medium to small scales due to the chaotic and ephemeral nature of features at these scales. The strong decline at the beginning of the spatial variances variance is due to small scale FTLE ridges features experiencing a strong and quick smoothing due to averaging, and slows down afterwards as mostly large scale FTLE ridges features are left. Robustness is particularly prominent at the larger spatial scales 7c, where little decay is noticed as more than 2-5 ensemble members are included in the average for large wavelengths. The spatial variance of \bar{F}_m stabilizes because large scales as the large scale features that are left in the system do not dissipate, are highly robust, whereas \bar{F}_t continues being smoothed at all scales due to FTLE ridge the formation, drift, deformation and dissipation of FTLE features happening at all scales.

4 Discussion Summary and discussion

Using ridges in FTLE fields as proxy, we see that LCS are variable across ensemble members and time. Potentially robust and persistent structures have been identified by averaging out the Features in ocean surface circulation, as described by FTLE analysis, have been investigated in terms of their persistence in time and robustness across EPS ensemble members. Statistics

475 of FTLE, in this study mainly limited to the mean, were computed to assess their variability. Both smaller-scale details and
large-scale features of the FTLE fields are variable over time and across ensemble members. Time and ensemble averages
have therefore been computed as an attempt to identify robust and persistent FTLE features, respectively, while averaging out
transient and uncertain features. In this section the following will be discussed: i) the persistence of FTLE ridges, ii) seasonality
and iii) robustness. Below we summarize and discuss some of the key findings.

480 4.1 Temporal variability FTLE as an indicator of Lagrangian Coherent Structures LCS and transport barriers

The flow field, and associated FTLE field, is seen to vary drastically over short time periods. Flow features that develop FTLE
ridges will drift, deform and dissipate over a range of time scales. The lifetime of a particular FTLE ridge is restricted by
the lifetime of the flow structure it represents. As a consequence, we expect that some LCS persist over time, particularly the
structures formed by large scale circulation as these typically imply longer time scales.

485 In the LoVe region, LCSs describe attracting and repelling properties of fluid flows, as well as define transport barriers
(Haller and Yuan, 2000; Farazmand and Haller, 2012; Haller, 2015). FTLE ridges are seen to frequently form along the continental
slope during winter. Particular FTLE ridges can be distinguished from \bar{F}_t for short time averages, but the smoothing ridges have
been discussed as possibly indicating the presence of LCSs, with clear limitations however. For instance, horizontal velocity
shear may produce large FTLE values but will not yield material convergence towards or divergence away from the FTLE
490 feature. Thus, such FTLE features are not indicative of LCSs (Haller, 2002; Branicki and Wiggins, 2010; Haller and Sapsis, 2011; Karrasch
). Other limitations exist, but a strength of the FTLE field increases with averaging time. The small scale FTLE ridges, being
more chaotic and short lived, are smoothed at the highest rate, whereas the large scale FTLE anomalies remain visible for
longer averaging times. Thus large scale structures are more persistent and mainly these define where \bar{F}_t indicate frequent
LCS activity, especially for longer time averages. approach is that it allows for simple statistical analysis of flow field features
495 that in some instances point to the existence of LCSs.

Permanent geomorphological features present a defining constraint on the ocean circulation, e.g. large scale bathymetry
steers ocean currents at high latitudes (Gille et al., 2004). Frequent FTLE ridges along At the very least, the systematic patterns
in the FTLE fields over the continental slope in the LoVe region are formed by the persistent topography-steered NCC and
NwAC. Dong et al. (2021) detected a persistent LCS transport barrier along the continental slope at LoVe. Our results are
500 based on a different time period, scale, and detection method, i.e. Dong et al. computed *repelling* LCSs using the Finite-Size
Lyapunov Exponent method from altimetry, which generally do off LoVe do suggest that the methods picks up important
dynamical features. The current system in the study region is strongly impacted by a steep continental slope, which sets up
a strong ambient potential vorticity (PV) gradient. As a result, a meandering current—guided by the bathymetry—will cause
a recurring FTLE pattern, with implications for both robustness and persistence. Dong et al. (2021) also identified persistent
505 FSLE in the LoVe region. Although FSLE generally does not coincide with the FTLE approach (Karrasch and Haller, 2013).
Furthermore, our velocity fields are of higher spatio-temporal resolution, hence detecting smaller and more transient structures.
Using time and ensemble average, however, we are able to find agreement with the structures detected by Dong et al. (2021).
Appropriate time or ensemble averaging enables retrieval of large scale transport barriers using high-resolution ocean models FTLE

(Karrasch and Haller, 2013), we find agreement in our results with Dong et al. (2021), who further showed that FSLE features hinder cross-slope transport. In other words, the FTLE and FSLE fields both seem to have detected a dynamical transport barrier (if not perfectly impenetrable) we know should exist from the ambient PV field.

A ~~weakness in time averaging of FTLE fields~~ caveat in analysing FTLE fields in terms of their average is that details in shape and direction of LCS are lost in \overline{F}_T . As discussed in Sec. 2.1, the average may consist of a few long, continuous long-lived FTLE ridges, which result in continuous transport barriers, or many short and transient ridges allowing for material exchange. Other methods for detecting persistent LCS could yield more nuanced results, individual FTLE ridges are lost. A ridge detection, that is the identification of what under ideal conditions will be LCS manifolds, could provide information on strain directionality, which may also be persistent under e.g. as used by Dong et al. (2021). The topographical current steering. Instead of averaging, one could follow a similar approach as Dong et al. (2021), where the authors defined a set of criterion for the existence of a ~~transport barrier~~ particular FSLE ridge and investigated the frequency ~~of the criterion being with which~~ the criterion was fulfilled. Another approach could be to select a particular FTLE ridge and study how it evolves over time. Its lifetime, propagation distance, growth/dissipation-rate and structural evolution could then be ~~studied~~. Possibly, a relation between that FTLE ridge size, strength ~~and its~~, and lifetime could be established.

~~Time~~ As mentioned above, there are other, improved, proxies for LCSs. Duran et al. (2018) proposes a method for computing the climatology of LCSs using a so-called quasi-steady LCS method, yielding information about LCS persistence over a selected time period. This method is tested in the Brazilian current by Gouveia et al. (2020), where the authors state that large-scale flow features give rise to persistent quasi-steady LCSs. Quasi-steady LCS allows for more direct extraction of transport barriers than FTLE ridges, and may therefore be better suited for investigating the long-term climatology of particle transport of e.g. nutrients. Seeing that the method described by Duran et al. (2018) handles time averages, we argue for the potential of finding robust LCS transport barriers by combining ensemble methods with quasi-steady LCS, and propose this as a topic for future study. Similarly to FTLEs, if quasi-steady LCSs prove to be robust, the method could be used in operational oceanography to provide forecasts about e.g. possible search-and-rescue regions.

4.2 Temporal variability of FTLE

The analyses above confirm that the flow and associated FTLE field are seen to vary drastically over short time periods. Flow features that develop pronounced structures in the FTLE field will drift, deform and vanish over a range of time scales. Clearly, the lifetime of a particular FTLE feature is restricted by the lifetime of the flow structure it represents. Specifically, features formed by large-scale circulation as these typically imply longer time scales.

Permanent geomorphological features present a defining constraint on the ocean circulation and, in particular, large-scale bathymetry steers ocean currents at high latitudes (Gille et al., 2004). In the LoVe region, the persistent topographically-steered NCC and NwAC give rise to frequent high-valued FTLE features along the continental slope during winter (Fig. 5a). Individual FTLE features are hard to detect from the monthly-averaged FTLE field, but may be distinguished for shorter time averages where the smoothing effect due to averaging is smaller. The small-scale FTLE features, being more chaotic and short lived, are

smoothed at the highest rate, whereas the large-scale FTLE anomalies remain visible for longer averaging times. Large-scale structures are expected to be more persistent.

545 Thus, time averaging of FTLE fields provides information about where FTLE ridges/features frequently form. Analysis of time-averaged FTLE and LCS is However, we note that strong values in the FTLE average may sometimes result from infrequent but very strong FTLE values. Analysis of time-averaged FTLE is therefore useful for identifying regions of material accumulation and entrainment. For instance, we expect that the semi-permanent anti-cyclonic eddy-Lofoten Vortex (Fig. 1) in the middle of the Lofoten Basin (Raj et al., 2015; Isachsen, 2015) forms persistent and re-occurring FTLE ridges Fig.8 will form persistent and re-occurring FTLE features (Fig. 8). Furthermore, the canyons in the LoVe region host a multitude of aquatic 550 organisms, e.g. cold water coral reefs, which is possible because of the nutrient accumulation here (Sundby et al., 2013; Bøe et al., 2016). We argue that these canyons will contribute to formation of persistent LCS/FTLE features, providing a control mechanism for particle transport towards specific locations.

4.3 Seasonal variability

Ocean currents in the LoVe region show seasonal variability in response to atmospheric forcing and seasonal hydrography. 555 Autumn the seasonally-varying hydrography. The autumn and winter months are characterized by westerly winds with transient low pressures passing pressure systems passing through the region, while spring and summer winds can be and the water pile-up against the coast accelerates the currents. Spring and summer, in contrast, are dominated by moderate easterly winds (Furnes and Sundby, 1981) During and weaker currents. In spring and summer, seasonal stratification sets as response the seasonal stratification also responds to freshwater runoff and solar radiation (Christensen et al., 2018). The associated- 560 The associated seasonal ocean circulation patterns are reflected in the FTLE fields -

Pronounced LCS develop in different locations during the seasons; FTLE ridges occur along (Fig. 5. Most pronounced is a clear difference in the intensity of the FTLE field over the continental slope during winter and closer to the coastline during summer. Seasonal. A well-mixed water column during winter results in more barotropic flow, hence the bathymetry controls winter circulation and high FTLE values develop in the lateral shear region along topography-following slope currents. In 565 contrast, seasonal stratification due to surface heating during summer leads to a partial decoupling of the ocean surface layer from deeper currents, thus bathymetry has a weaker impact on both robustness and persistence of surface flow structures during summer. A well-mixed water column during winter results in more barotropic flow, hence the bathymetry controls winter circulation and FTLE ridges develop in the lateral shear region along topography-following slope currents. Note that FTLE ridges and transport barriers Note that pronounced FTLE features may occur along the continental slope can still occur 570 in summer, but seem to have a smaller impact on transport these are less typical or weak, therefore tend to be washed out in both time and ensemble averages.

The coastline is expected to have a similar impact on FTLE formation throughout the year, as it directly affects surface currents, although near-shore FTLEs are suspected of mainly being produced by horizontal velocity shear. However, around Moskstraumen (Figs. 1 and 5) we identify-identified higher FTLE variability in summer that is tied to tidal pumping through

575 the narrow sound. Surface-intensified flow as a consequence of distinct summer stratification may amplify surface currents in this particular location (Sperrevik et al., 2017).

~~The higher LCS activity during winter may be connected~~ Finally, higher FTLE values during winter can be expected to be related to more energetic flows at the scales of 1-100km ~~scale during this season. These flows are~~. Circulation at this scale is intensified by baroclinic instabilities formed around geostrophic eddies, and are much stronger during winter than in summer (Callies et al., 2015).

4.4 Uncertainty of FTLEs in realistic flow fields

Ocean current uncertainty stems from non-linear equations of motion: small errors in initial ~~conditions or boundary conditions, as well as tunable parameter values, can~~ cause large errors in numerical integrations (Lorenz, 1963), ~~and error propagation may cause large impact~~. Error propagation may thus have impacts in trajectory simulations (e.g. Zimmerman, 1986; de Aguiar et al., 2023). By this argument ~~uncertainty in LCS estimates, uncertainties in FTLE fields~~ derived from uncertain ~~current fields is expected~~. In addition, ~~currents are expected~~. Allshouse et al. (2017) discussed uncertainty from the impact of wind drag on surface ~~LCS must be expected for realistic drift applications (Allshouse et al., 2017). The FTLEs~~. In addition, we discuss the uncertainty due the flow field itself. A regional scale ocean EPS, Barents-2.5 ~~EPS used in this study~~, is here used to describes uncertainties of ocean currents in the analysis and throughout the forecast range, ~~with the notion that most extreme velocities are slightly underestimated~~ (Idžanović et al., 2023). By calculating FTLE ~~'s fields~~ for each ensemble member, we propagate the ocean model uncertainty into the ~~LCS FTLE~~ analysis presented here. ~~We see that variability in FTLE ridges occur both positionally and structurally between members. FTLE ridges~~ The various members exhibit differences in the FTLE fields, e.g. in terms of feature location, intensity and shape. Generally, FTLE features that exist in only one or few members are statistically unlikely to ~~exists~~ exist (compare Fig. 6), emphasizing the need of an EPS when employing ~~LCS FTLE~~ in operational oceanography.

Ensemble averaging is here suggested as a method to detect robust ~~LCSs~~ FTLE features, i.e. ~~FTLE ridges features~~ that appear in a majority of members and can therefore be considered likely to exist, despite uncertainties in the underlying flow. Similarly to the time average, the ensemble average smooths out ~~FTLE ridges resulting in regions where these are more likely to form~~ distinct features in the FTLE field, resulting in an average FTLE field \bar{F}_m that highlights only the most predictable features. Some FTLE ~~ridges features~~ can still be distinguished in \bar{F}_m , even after considering all 24 ensemble members of the Barents-2.5 EPS (Fig. ??7). In particular, ~~FTLE ridges situated~~ high FTLE areas located along the continental slope tend to be more robust. ~~The~~ As discussed above, the steep bathymetry plays an important role in ~~forming robust FTLEs~~ causing the robustness, because even though the surface currents themselves are uncertain, the bathymetry constrains surface currents equally across the ensemble.

605 The spectral analysis (Fig. ??) ~~showed that large scale~~ 7) confirmed our expectations that large-scale FTLE features are more robust FTLEs, as variability does not decay at ~~low wavenumbers when increasing large wavelengths when increasing the~~ number of ensemble members in the averaging. ~~Smaller scale features are also present each individual member, but these beyond 2-4 members. Small-scale features, however,~~ are effectively removed by the ensemble average. ~~Small scale flows~~

610 because they are more chaotic and ~~exhibits exhibiting~~ lower predictability. ~~In the LoVe region, large-scale eddies exist in~~
~~the majority of the Barents-2.5 EPS members. Individual FTLE ridges formed by these larger-scale eddies are seen to vary~~
~~between members, however, these can still be distinguished in the ensemble average \overline{F}_m . We conclude that FTLE ridges~~
~~associated with larger-scale~~ The conclusion is that FTLE features associated with larger-scale flows are more robust than small
scale FTLEs ~~formed by more chaotic flows.~~

615 Sensitivity of the FTLE method has previously been investigated using satellite altimetry products by Harrison and Glatz-
maier (2012) ~~and Badza et al. (2023). Both studies concluded,~~ where the authors conclude that FTLEs are fairly insensitive to
noise included in the velocity fields. ~~Harrison and Glatzmaier (2012) finds and~~ that FTLEs are robust for ~~large-scale~~ large-scale
eddies and strong jets, ~~whereas Badza et al. (2023) observes smoothing of the FTLE field due to ensemble averaging and~~
~~consistency between FTLE fields across an ensemble. In addition, (Gouveia et al., 2020) argue that persistent large-scale feature~~
Gouveia et al. (2020) argues that persistent large-scale features in particular give rise to quasi-steady LCS, such as the feature
620 reported by ~~(Dong et al., 2021) Dong et al. (2021)~~ Dong et al. (2021) which is also ~~analysed analyzed~~ in our study. In addition to time-persistent
features, we investigate ~~LCS detections~~ FTLE detection from transient flow features. ~~The~~ Importantly, the Barents-2.5 EPS
model used in this study can represent smaller and more transient structures than the aforementioned satellite products, ~~and we~~
~~can argue that FTLEs.~~ From this we found that high FTLE areas are more uncertain at smaller scales, but robust ~~of~~ where the
flow is constrained by coastal or bathymetric steering.

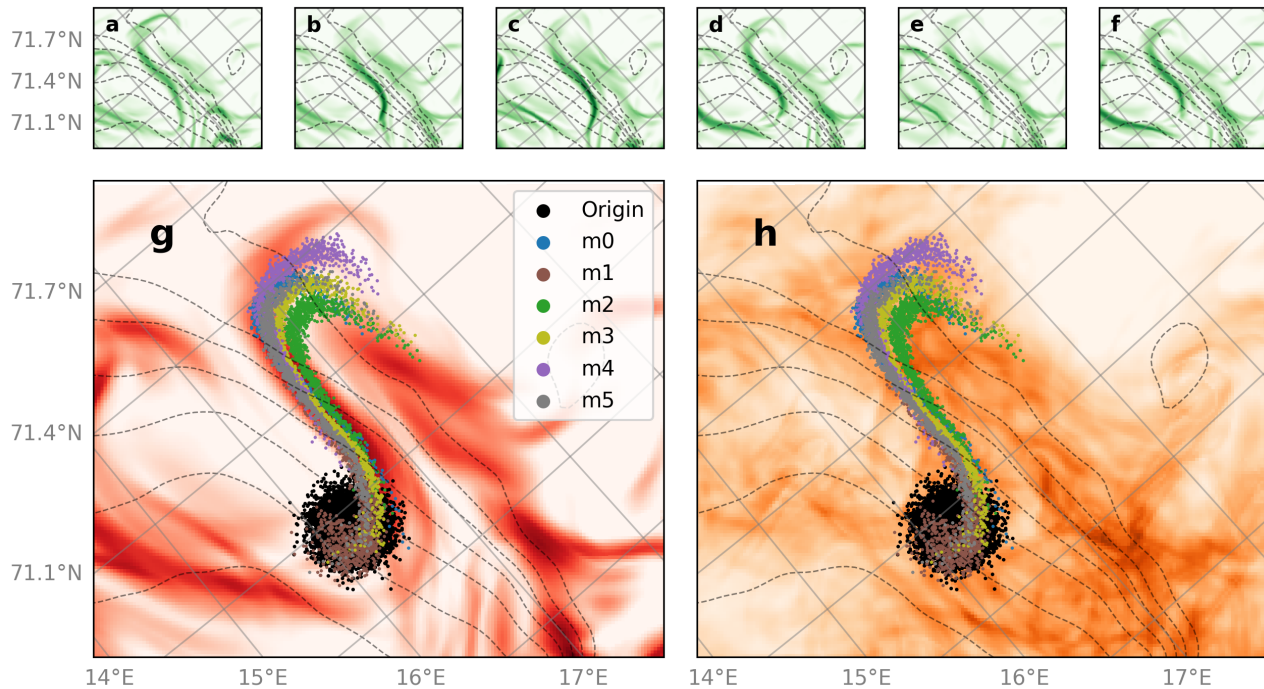
Operational forecasting

Figure 8. FTLE averages and particle clusters advected using velocity fields from a small number of different Barents-2.5 EPS ensemble members. Panels a-f show the 24-hour FTLE fields from each member used to advect the particles, while panels g and h show the ensemble averaged FTLE field and the monthly averaged FTLE field from one member, respectively. Black dots in panels g and h mark the initial position of the particles on 2023-01-01, and their final positions after four days.

Operational use of LCS-FTLE analysis in forecasting, e.g. for search-and-rescue, oil-spill operations or path-planning (e.g. Beegle-Krause et al., 2011; Ramos et al., 2018; Serra et al., 2020), should be viewed together with the uncertainty in context of the uncertainty in ocean current predictions. LCSs can yield the much needed information about material accumulation regions and transport barriers, which could prove vital for saving lives or mitigate environmental catastrophes. Although FTLE ridges And although FTLE fields are variable across an ensemble, we see that some FTLE ridges have seen that some features of the FTLE field are more robust than others. An ensemble of FTLE must FTLEs must thus be assessed to separate robust from non-robust appearance of flow features. A robust FTLE ridge detection presents features. The detection of a robust FTLE feature would thus present an opportunity to accurately identify search regions and dispatch environmental clean-up resources.

635 The ensemble average is efficient at reducing the FTLE features in presumably unpredictable parts of the flow field, whereas some Fig 8 illustrates the power of ensemble averaging. It shows a situation where there happens to be high agreement between

particle cluster trajectories over four days from a few different, randomly selected, ensemble realizations. The ensemble-averaged FTLE field over all 24 ensemble members is also shown and appears to be highly robust: FTLE features remain very strong and clearly articulated in the FTLE ensemble average. These are the features we expect to be good predictors of actual LCSs average. More importantly, particle clusters from all ensemble members are seen to be attracted towards the nearby high values of \bar{F}_m . Thus, in such a case, the ensemble-averaged FTLE field provides a clear added value to trajectory forecasting in a real-time setting.

Distinct FTLE ridges remain visible in short time averages (Fig.4). The time average effectively removes short-lived FTLE ridges over longer time period, but keeps them for short time averages (Fig. ??). LCSs could therefore be used for short term forecasting. In contrast to this, the 30-day FTLE average from a single ensemble member, shown in Fig. 8, does not shed much light on the short-term particle trajectories in this particular situation. This should not come as a surprise, as the FTLE features will have evolved substantially over the month. It is likely that certain FTLE features may be distinguished in shorter-term averages, taken over e.g. three days, knowing that most small-scale and short-lived LCSs also persist at this forecasting length.

Process studies on particle transport

The continental shelf sea off LoVe is known to be a hot spot for fisheries due to its high nutrient concentrations, forming feeding grounds and spawning banks for marine life (Sundby and Bratland, 1987; Sundby et al., 2013). The transport of relevant nutrients and material in this region is widely studied (e.g. Adlandsvik and Sundby, 1994; Röhrs et al., 2014). The LCS analysis presented here shed light on an additional mechanism for enabling cross-slope transport of nutrients that could play a role in sustaining biological production during summer, when nutrient levels in the photic layer are generally consumed following the spring bloom. As an example, important zooplankton sustaining fish stocks at LoVe, *Calanus Finmarchicus*, overwinters at deeper depths off the continental shelf (Kaartvedt, 1996) and may be transported onto the continental shelf. The existence of persistent LCS transport barriers may hinder cross-slope transport during winter. Applying LCSs to different regions may reveal important transport barriers and material accumulation zones with high impact on local biology, and may be utilized to identify regions of high biological production (Johnsen et al., 2024) 3–4 days, could be utilized for short-term forecasting. However, in that case it may be more appropriate to compute the FTLE field with $T = 3$ days instead, then obtaining the ensemble-averaged FTLE field over the time interval.

5 Conclusions

LCS-FTLEs are clearly imperfect representations of LCSs. And yet, FTLE analysis provides a practical diagnostic tool for describing the particle transport in uncertain velocity fields. We show that analyzing how ocean flow morphology associated with deformation impacts particle transport. In this numerical model study we have examined how the uncertainty of ocean model forecasts propagate into the, illustrated in an ocean EPS, propagates into FTLE fields. By employing time and It was shown that by employing ensemble averaging of ensemble FTLE fields, certain LCS-detections robust features of the FTLE field, that is features which the EPS system has gotten right in a statistical sense, may be separated from uncertain, non-robust,

features. In particular, ensemble averaging typically retains flow structures at larger scales that are time-evolving, but pre-
670 dictable at specific times. ~~These~~ The averaging will more typically wash out FTLE structures present in individual ensemble
members, but it still has the potential to highlight regions over which FTLE features are statistically likely to emerge. Such
features are often influenced by geomorphological ~~constraint, or related to large-scale circulation patterns~~ constraints which,
in our specific study region, was exemplified by a steep continental slope that imposes strong—and permanent—ambient PV
gradients. We have also shown how such permanent environmental constraints can make FTLE fields persistent in time. Large
675 seasonal ~~differences in LCSs due to changes in weather and ocean conditions are observed. Because of flow field evolution,~~
~~LCSs are~~ variations in atmospheric forcing and hydrographic conditions can impact both the robustness and persistence of
FLTE structures, but the FTLE fields studied here were generally shown to be more robust than persistent. ~~LCS analysis adds~~
So the over-all lesson learned from the study is that FTLE analysis can indeed add value to operational forecasting ~~only where~~
~~these are robust, which can be judged by combining LCS analysis with ensemble prediction methods, even in light of the~~
680 highly nonlinear and chaotic nature of real ocean flows. The key requirement is the forecast is treated as a probabilistic one,
most practically produced using ensemble techniques.

Code and data availability. Archived data from the operational model runs of Barents-2.5 are disseminated on https://thredds.met.no/thredds/fou-hi/barents_eps.html (Norwegian Meteorological Institute). Software for computing FTLE fields can be found on <https://github.com/mateuszmatu/LCS> (Matuszak, 2024).

685 *Author contributions.* FTLE analysis: MM. Seasonal analysis: MM, PEI. Circulation model: MI, JR. Manuscript preparation: MM, JR, PEI, MI. Study concept: JR.

Competing interests. We declare absence of competing interests related to this work.

Acknowledgements. We acknowledge funding by the Research Council of Norway through ~~grant nos. grants~~ [237906 \(CIRFA\)](#) ~~and~~ [300329 \(EcoPulse\)](#) ~~and~~ [314826 \(TopArctic\)](#).

690 References

- Adlandsvik, B. and Sundby, S.: Modelling the transport of cod larvae from the Lofoten area, ICES Marine Science Symposia, 198, 379–392, 1994.
- Allshouse, M. R., Ivey, G. N., Lowe, R. J., Jones, N. L., Beegle-Krause, C. J., Xu, J., and Peacock, T.: Impact of windage on ocean surface Lagrangian coherent structures, *Environmental Fluid Mechanics*, 17, 473–483, <https://doi.org/10.1007/s10652-016-9499-3>, 2017.
- 695 Badza, A., Mattner, T. W., and Balasuriya, S.: How sensitive are Lagrangian coherent structures to uncertainties in data?, *Physica D: Nonlinear Phenomena*, 444, 133–158, <https://doi.org/10.1016/j.physd.2022.133580>, 2023.
- Balasuriya, S.: Explicit invariant manifolds and specialised trajectories in a class of unsteady flows, *Physics of Fluids*, 24, 127–101, <https://doi.org/10.1063/1.4769979>, 2012.
- Balasuriya, S.: Uncertainty in finite-time Lyapunov exponent computations, *Journal of Computational Dynamics*, 7, 313–337, 700 <https://doi.org/10.3934/jcd.2020013>, 2020.
- Balasuriya, S., Kalampattel, R., and Ouellette, N. T.: Hyperbolic neighbourhoods as organizers of finite-time exponential stretching, *Journal of Fluid Mechanics*, 807, 509–545, <https://doi.org/10.1017/jfm.2016.633>, 2016.
- Beegle-Krause, C. J., Peacock, T., and Allshouse, M.: Exploiting Lagrangian coherent structures (LCS) for the calculation of oil spill and search-and-rescue drift patterns in the ocean, <https://www.osti.gov/etdweb/biblio/21547684>, 2011.
- 705 Branicki, M. and Wiggins, S.: Finite-time Lagrangian transport analysis: stable and unstable manifolds of hyperbolic trajectories and finite-time Lyapunov exponents, *Nonlinear Processes in Geophysics*, 17, 1–36, <https://doi.org/10.5194/npg-17-1-2010>, 2010.
- Brunton, S. L. and Rowley, C. W.: Fast computation of finite-time Lyapunov exponent fields for unsteady flows, *Chaos: An Interdisciplinary Journal of Nonlinear Science*, 20, 017–503, <https://doi.org/10.1063/1.3270044>, 2010.
- Bøe, R., Bellec, V. K., Dolan, M. F. J., Buhl-Mortensen, P., Rise, L., and Buhl-Mortensen, L.: Cold-water coral reefs in the Hola glacial 710 trough off Vesterålen, North Norway, *Geological Society, London, Memoirs*, 46, 309–310, <https://doi.org/10.1144/M46.8>, 2016.
- Børve, E., Isachsen, P. E., and Nøst, O. A.: Rectified tidal transport in Lofoten–Vesterålen, northern Norway, *Ocean Science*, 17, 1753–1773, <https://doi.org/10.5194/os-17-1753-2021>, 2021.
- Callies, J., Callies, J., Ferrari, R., Klymak, J. M., and Gula, J.: Seasonality in submesoscale turbulence, *Nature communications*, 6, 6862, <https://doi.org/10.1038/ncomms7862>, 2015.
- 715 Chen, G. and Han, G.: Contrasting Short-Lived With Long-Lived Mesoscale Eddies in the Global Ocean, *Journal of Geophysical Research: Oceans*, 124, 3149–3167, <https://doi.org/10.1029/2019JC014983>, 2019.
- Christensen, K. H., Sperrevik, A. K., and Broström, G.: On the Variability in the Onset of the Norwegian Coastal Current, *Journal of Physical Oceanography*, 48, 723 – 738, <https://doi.org/10.1175/JPO-D-17-0117.1>, 2018.
- Dagestad, K.-F. and Röhrs, J.: Prediction of ocean surface trajectories using satellite derived vs. modeled ocean currents, *Remote Sensing of 720 Environment*, 223, 130–142, <https://doi.org/10.1016/j.rse.2019.01.001>, 2019.
- Dagestad, K.-F., Röhrs, J., Breivik, Ø., and Ådlandsvik, B.: OpenDrift v1.0: a generic framework for trajectory modelling, *Geoscientific Model Development*, 11, 1405–1420, <https://doi.org/10.5194/gmd-11-1405-2018>, 2018a.
- Dagestad, K.-F., Röhrs, J., Breivik, O., and Ådlandsvik, B.: OpenDrift v1.0: a generic framework for trajectory modelling, *Geoscientific Model Development*, 11, 1405–1420, <https://doi.org/10.5194/gmd-11-1405-2018>, 2018b.
- 725 de Aguiar, V., Röhrs, J., Johansson, A. M., and Eltoft, T.: Assessing ocean ensemble drift predictions by comparison with observed oil slicks, *Frontiers in Marine Science*, 10, <https://doi.org/10.3389/fmars.2023.1122192>, 2023.

- Denis, B., Côté, J., and Laprise, R.: Spectral Decomposition of Two-Dimensional Atmospheric Fields on Limited-Area Domains Using the Discrete Cosine Transform (DCT), *Monthly Weather Review*, 130, 1812 – 1829, [https://doi.org/10.1175/1520-0493\(2002\)130<1812:SDOTDA>2.0.CO;2](https://doi.org/10.1175/1520-0493(2002)130<1812:SDOTDA>2.0.CO;2), 2002.
- 730 Dong, H., Zhou, M., Hu, Z., Zhang, Z., Zhong, Y., Basedow, S. L., and Smith Jr., W. O.: Transport Barriers and the Retention of *Calanus finmarchicus* on the Lofoten Shelf in Early Spring, *Journal of Geophysical Research: Oceans*, 126, e2021JC017408, <https://doi.org/10.1029/2021JC017408>, 2021.
- d'Ovidio, F., Fernández, V., Hernández-García, E., and López, C.: Mixing structures in the Mediterranean Sea from finite-size Lyapunov exponents, *Geophysical Research Letters*, 31, <https://doi.org/10.1029/2004GL020328>, 2004.
- 735 Duran, R., Beron-Vera, F., and Olascoaga, M.: Extracting quasi-steady Lagrangian transport patterns from the ocean circulation: An application to the Gulf of Mexico, *Scientific reports*, 8, 5218, <https://doi.org/10.1038/s41598-018-23121-y>, 2018.
- Evensen, G.: Inverse methods and data assimilation in nonlinear ocean models, *Physica D: Nonlinear Phenomena*, 77, 108–129, [https://doi.org/10.1016/0167-2789\(94\)90130-9](https://doi.org/10.1016/0167-2789(94)90130-9), 1994.
- Farazmand, M. and Haller, G.: Computing Lagrangian coherent structures from their variational theory, *Chaos: An Interdisciplinary Journal of Nonlinear Science*, 22, 013 128, <https://doi.org/10.1063/1.3690153>, 2012.
- 740 Furnes, G. and Sundby, S.: Upwelling and wind induced circulation in Vestfjorden, The Norwegian Coastal Current, *Proceedings from the Norwegian Coastal Current Symposium*, 1, 152–177, 1981.
- Gascard, J.-C., Raisbeck, G., Sequeira, S., Yiou, F., and Mork, K. A.: The Norwegian Atlantic Current in the Lofoten basin inferred from hydrological and tracer data (129I) and its interaction with the Norwegian Coastal Current, *Geophysical Research Letters*, 31, <https://doi.org/10.1029/2003GL018303>, 2004.
- 745 Ghosh, A., Suara, K., McCue, S. W., Yu, Y., Soomere, T., and Brown, R. J.: Persistency of debris accumulation in tidal estuaries using Lagrangian coherent structures, *Science of The Total Environment*, 781, 146 808, <https://doi.org/10.1016/j.scitotenv.2021.146808>, 2021.
- Gille, S., Metzger, J., and Tokmakian, R.: Seafloor Topography and Ocean Circulation, *Oceanography*, 17, 47–54, <https://doi.org/10.5670/oceanog.2004.66>, 2004.
- 750 Giudici, A., Suara, K. A., Soomere, T., and Brown, R.: Tracking areas with increased likelihood of surface particle aggregation in the Gulf of Finland: A first look at persistent Lagrangian Coherent Structures (LCS), *Journal of Marine Systems*, 217, 103 514, <https://doi.org/https://doi.org/10.1016/j.jmarsys.2021.103514>, 2021.
- Gouveia, M. B., Duran, R., Lorenzetti, J. A., Assireu, A. T., Toste, R., Assad, L. P. d. F., and Gherardi, D. F. M.: Persistent meanders and eddies lead to a quasi-steady Lagrangian transport pattern in a weak western boundary current, *Scientific reports*, <https://doi.org/10.48550/arXiv.2008.07620>, 2020.
- 755 Guo, H., He, W., Peterka, T., Shen, H.-W., Collis, S. M., and Helmus, J. J.: Finite-Time Lyapunov Exponents and Lagrangian Coherent Structures in Uncertain Unsteady Flows, *IEEE Transactions on Visualization and Computer Graphics*, 22, 1672–1682, <https://doi.org/10.1109/TVCG.2016.2534560>, 2016.
- Hadjighasem, A., Farazmand, M., Blazeovski, D., Froyland, G., and Haller, G.: A critical comparison of Lagrangian methods for coherent structure detection, *Chaos: An Interdisciplinary Journal of Nonlinear Science*, 27, 053 104, <https://doi.org/10.1063/1.4982720>, 2017.
- 760 Haller, G.: Distinguished material surfaces and coherent structures in three-dimensional fluid flows, *Physica D: Nonlinear Phenomena*, 149, 248–277, [https://doi.org/10.1016/S0167-2789\(00\)00199-8](https://doi.org/10.1016/S0167-2789(00)00199-8), 2001.
- Haller, G.: Lagrangian coherent structures from approximate velocity data, *Physics of Fluids*, 14, 1851–1861, <https://doi.org/10.1063/1.1477449>, 2002.

- 765 Haller, G.: A variational theory of hyperbolic Lagrangian Coherent Structures, *Physica D: Nonlinear Phenomena*, 240, 574–598, <https://doi.org/10.1016/j.physd.2010.11.010>, 2011.
- Haller, G.: Lagrangian Coherent Structures, *Annual Review of Fluid Mechanics*, 47, 137–162, <https://doi.org/10.1146/annurev-fluid-010313-141322>, 2015.
- Haller, G. and Sapsis, T.: Lagrangian coherent structures and the smallest finite-time Lyapunov exponent, *Chaos: An Interdisciplinary Journal of Nonlinear Science*, 21, 023 115, <https://doi.org/10.1063/1.3579597>, publisher: American Institute of Physics, 2011.
- 770 Haller, G. and Yuan, G.: Lagrangian coherent structures and mixing in two-dimensional turbulence, *Physica D: Nonlinear Phenomena*, 147, 352–370, [https://doi.org/10.1016/S0167-2789\(00\)00142-1](https://doi.org/10.1016/S0167-2789(00)00142-1), 2000.
- Harrison, C. S. and Glatzmaier, G. A.: Lagrangian coherent structures in the California Current System – sensitivities and limitations, *Geophysical & Astrophysical Fluid Dynamics*, 106, 22–44, <https://doi.org/10.1080/03091929.2010.532793>, 2012.
- 775 Hussain, A. K. M. F.: Coherent structures—reality and myth, *The Physics of Fluids*, 26, 2816–2850, <https://doi.org/10.1063/1.864048>, 1983.
- Idžanović, M., Rikardsen, E. S. U., and Röhrs, J.: Forecast uncertainty and ensemble spread in surface currents from a regional ocean model, *Frontiers in Marine Science*, 10, <https://doi.org/10.3389/fmars.2023.1177337>, 2023.
- Isachsen, P. E.: Baroclinic instability and the mesoscale eddy field around the Lofoten Basin, *Journal of Geophysical Research: Oceans*, 120, 2884–2903, <https://doi.org/10.1002/2014JC010448>, 2015.
- 780 Johnsen, I. A., Röhrs, J., and Kutti, T.: Exploring the role of food delivery mechanisms in regulating the distribution of the cold water coral *Lophelia pertusa*, manuscript in preparation, 2024.
- Kaartvedt, S.: Habitat preference during overwintering and timing of seasonal vertical migration of *Calanus finmarchicus*, *Ophelia*, 44, 145–156, <https://doi.org/10.1080/00785326.1995.10429844>, 1996.
- Karrasch, D. and Haller, G.: Do Finite-Size Lyapunov Exponents detect coherent structures?, *Chaos: An Interdisciplinary Journal of Nonlinear Science*, 23, 043 126, <https://doi.org/10.1063/1.4837075>, 2013.
- 785 Koszalka, I., LaCasce, J. H., and Mauritzen, C.: In pursuit of anomalies—Analyzing the poleward transport of Atlantic Water with surface drifters, *Deep Sea Research Part II: Topical Studies in Oceanography*, 85, 96–108, <https://doi.org/10.1016/j.dsr2.2012.07.035>, 2013.
- Krishna, K., Brunton, S. L., and Song, Z.: Finite Time Lyapunov Exponent Analysis of Model Predictive Control and Reinforcement Learning, <https://arxiv.org/abs/2304.03326>, 2023.
- 790 Lebreton, L. C. M., Greer, S. D., and Borrero, J. C.: Numerical modelling of floating debris in the world’s oceans, *Marine Pollution Bulletin*, 64, 653–661, <https://doi.org/10.1016/j.marpolbul.2011.10.027>, 2012.
- Lee, Y.-K., Shih, C., Tabeling, P., and Ho, C.-M.: Experimental study and nonlinear dynamic analysis of time-periodic micro chaotic mixers, *Journal of Fluid Mechanics*, 575, 425–448, <https://doi.org/10.1017/S0022112006004289>, 2007.
- Lekien, F., Coulliette, C., Mariano, A. J., Ryan, E. H., Shay, L. K., Haller, G., and Marsden, J.: Pollution release tied to invariant manifolds: A case study for the coast of Florida, *Physica D: Nonlinear Phenomena*, 210, 1–20, <https://doi.org/10.1016/j.physd.2005.06.023>, 2005.
- 795 Leutbecher, M. and Palmer, T.: Ensemble forecasting, <https://doi.org/10.21957/c0hq4yg78>, 2007.
- Lorenz, E. N.: Deterministic Nonperiodic Flow, *Journal of Atmospheric Sciences*, 20, 130 – 141, [https://doi.org/10.1175/1520-0469\(1963\)020<0130:DNF>2.0.CO;2](https://doi.org/10.1175/1520-0469(1963)020<0130:DNF>2.0.CO;2), 1963.
- Lou, Q., Li, Z., Zhang, X., Xiang, X., and Cao, Z.: Lagrangian analysis of material transport around the headland in the Yellow River Estuary, *Frontiers in Marine Science*, 9, <https://doi.org/10.3389/fmars.2022.999367>, 2022.
- 800 Matuszak, M.: `matuszmatu/LCS: FTLE computation software` release for article, <https://doi.org/10.5281/zenodo.10797134>, 2024.

- Mitchelson-Jacob, G. and Sundby, S.: Eddies of Vestfjorden, Norway, *Continental Shelf Research*, 21, 1901–1918, [https://doi.org/10.1016/S0278-4343\(01\)00030-9](https://doi.org/10.1016/S0278-4343(01)00030-9), 2001.
- Müller, M., Homleid, M., Ivarsson, K.-I., Kjøltzow, M. A. O., Lindskog, M., Midtbø, K. H., Andrae, U., Aspelién, T., Berggren, L., Bjørge, D., Dahlgren, P., Kristiansen, J., Randriamampianina, R., Ridal, M., and Vignes, O.: AROME-MetCoOp: A Nordic Convective-Scale Operational Weather Prediction Model, *Weather and Forecasting*, 32, 609–627, <https://doi.org/10.1175/WAF-D-16-0099.1>, 2017.
- Norwegian Meteorological Institute: Barents-2.5 ocean and ice forecast model archive, [data set] last access 2024-04-29, https://thredds.met.no/thredds/fou-hi/barents_eps.html.
- Olascoaga, M. J. and Haller, G.: Forecasting sudden changes in environmental pollution patterns, *Proceedings of the National Academy of Sciences*, 109, 4738–4743, <https://doi.org/10.1073/pnas.1118574109>, 2012.
- Olascoaga, M. J., Rypina, I. I., Brown, M. G., Beron-Vera, F. J., Koçak, H., Brand, L. E., Halliwell, G. R., and Shay, L. K.: Persistent transport barrier on the West Florida Shelf, *Geophysical Research Letters*, 33, <https://doi.org/https://doi.org/10.1029/2006GL027800>, 2006.
- Peacock, T. and Haller, G.: Lagrangian coherent structures: The hidden skeleton of fluid flows, *Physics Today*, 66, 41–47, <https://doi.org/10.1063/PT.3.1886>, 2013.
- Peng, J. and Dabiri, J. O.: The ‘upstream wake’ of swimming and flying animals and its correlation with propulsive efficiency, *Journal of Experimental Biology*, 211, 2669–2677, <https://doi.org/10.1242/jeb.015883>, 2008.
- Pierrehumbert, R. T. and Yang, H.: Global Chaotic Mixing on Isentropic Surfaces, *Journal of the Atmospheric Sciences*, 50, 2462–2480, [https://doi.org/10.1175/1520-0469\(1993\)050<2462:GCMOIS>2.0.CO;2](https://doi.org/10.1175/1520-0469(1993)050<2462:GCMOIS>2.0.CO;2), 1993.
- Raj, R. P., Chafik, L., Nilsen, J. E. O., Eldevik, T., and Halo, I.: The Lofoten Vortex of the Nordic Seas, *Deep Sea Research Part I: Oceanographic Research Papers*, 96, 1–14, <https://doi.org/10.1016/j.dsr.2014.10.011>, 2015.
- Ramos, A. G., García-Garrido, V. J., Mancho, A. M., Wiggins, S., Coca, J., Glenn, S., Schofield, O., Kohut, J., Aragon, D., Kerfoot, J., Haskins, T., Miles, T., Haldeman, C., Strandkov, N., Allsup, B., Jones, C., and Shapiro, J.: Lagrangian coherent structure assisted path planning for transoceanic autonomous underwater vehicle missions, *Scientific Reports*, 8, 4575, <https://doi.org/10.1038/s41598-018-23028-8>, 2018.
- Rosenstein, M. T., Collins, J. J., and De Luca, C. J.: A practical method for calculating largest Lyapunov exponents from small data sets, *Physica D: Nonlinear Phenomena*, 65, 117–134, [https://doi.org/10.1016/0167-2789\(93\)90009-P](https://doi.org/10.1016/0167-2789(93)90009-P), 1993.
- Rosby, T., Ozhigin, V., Ivshin, V., and Bacon, S.: An isopycnal view of the Nordic Seas hydrography with focus on properties of the Lofoten Basin, *Deep Sea Research Part I: Oceanographic Research Papers*, 56, 1955–1971, <https://doi.org/10.1016/j.dsr.2009.07.005>, 2009.
- Röhrs, J., Christensen, K. H., Vikebø, F., Sundby, S., Saetra, O., and Broström, G.: Wave-induced transport and vertical mixing of pelagic eggs and larvae, *Limnology and Oceanography*, 59, 1213–1227, <https://doi.org/10.4319/lo.2014.59.4.1213>, 2014.
- Röhrs, J., Sutherland, G., Jeans, G., Bedington, M., Sperrevik, A. K., Dagestad, K.-F., Gusdal, Y., Mauritzen, C., Dale, A., and LaCasce, J. H.: Surface currents in operational oceanography: Key applications, mechanisms, and methods, *Journal of Operational Oceanography*, 0, 1–29, <https://doi.org/10.1080/1755876X.2021.1903221>, 2021.
- Röhrs, J., Gusdal, Y., Rikardsen, E., Duran Moro, M., Brændshøi, J., Kristensen, N. M., Fritzner, S., Wang, K., Sperrevik, A. K., Idžanović, M., Lavergne, T., Debernard, J., and Christensen, K. H.: Barents-2.5km v2.0: An operational data-assimilative coupled ocean and sea ice ensemble prediction model for the Barents Sea and Svalbard, *Geoscientific Model Development Discussions*, pp. 1–31, <https://doi.org/10.5194/gmd-2023-20>, 2023.
- Sakov, P., Counillon, F., Bertino, L., Lisæter, K. A., Oke, P. R., and Korablev, A.: TOPAZ4: an ocean-sea ice data assimilation system for the North Atlantic and Arctic, *Ocean Science*, 8, 633–656, <https://doi.org/10.5194/os-8-633-2012>, 2012.

- 840 Samelson, R.: Lagrangian Motion, Coherent Structures, and Lines of Persistent Material Strain, *Annual Review of Marine Science*, 5, 137–163, <https://doi.org/10.1146/annurev-marine-120710-100819>, 2013.
- Serra, M., Sathe, P., Rypina, I., Kirincich, A., Ross, S. D., Lermusiaux, P., Allen, A., Peacock, T., and Haller, G.: Search and rescue at sea aided by hidden flow structures, *Nature Communications*, 11, 2525, <https://doi.org/10.1038/s41467-020-16281-x>, 2020.
- Shadden, S. C., Lekien, F., and Marsden, J. E.: Definition and properties of Lagrangian coherent structures from finite-time Lyapunov exponents in two-dimensional aperiodic flows, *Physica D: Nonlinear Phenomena*, 212, 271–304, <https://doi.org/10.1016/j.physd.2005.10.007>, 845 2005.
- Shchepetkin, A. F. and McWilliams, J. C.: The regional oceanic modeling system (ROMS): a split-explicit, free-surface, topography-following-coordinate oceanic model, *Ocean Modelling*, 9, 347–404, <https://doi.org/10.1016/j.ocemod.2004.08.002>, 2005.
- Sperrevik, A. K., Röhrs, J., and Christensen, K. H.: Impact of data assimilation on Eulerian versus Lagrangian estimates of upper ocean transport, *Journal of Geophysical Research: Oceans*, 122, 5445–5457, <https://doi.org/10.1002/2016JC012640>, 2017.
- 850 Sundby, S.: Influence of bottom topography on the circulation at the continental shelf off northern Norway, *Fiskeridirektoratets Skrifter Serie Havundersokelser*, 17, 501–519, 1984.
- Sundby, S. and Bratland, P.: Spatial distribution and production of eggs from Northeast-arctic cod at the coast of Northern Norway 1983–1985, *Fisken og havet*, 1, 1987.
- Sundby, S., Fossum, P., Sandvik, A. D., Vikebø, F., Aglen, A., Buhl-Mortensen, L., Folkvord, A., Bakkeplass, K., Buhl-Mortensen, P., 855 Johannessen, M., Jørgensen, M. S., Kristiansen, T., Landra, C. S., Myksvoll, M. S., and Nash, R. D. M.: KunnskapsInnhenting Barantshavet–Lofoten–Vesterålen (KILO), 188 s., <https://imr.brage.unit.no/imr-xmlui/handle/11250/113923>, publisher: Havforskningsinstituttet, last access: 17 April 2024, 2013.
- Søiland, H. and Rossby, T.: On the structure of the Lofoten Basin Eddy, *Journal of Geophysical Research: Oceans*, 118, 4201–4212, <https://doi.org/https://doi.org/10.1002/jgrc.20301>, 2013.
- 860 Tang, W., Chan, P. W., and Haller, G.: Accurate extraction of Lagrangian coherent structures over finite domains with application to flight data analysis over Hong Kong International Airport, *Chaos: An Interdisciplinary Journal of Nonlinear Science*, 20, 017502, <https://doi.org/10.1063/1.3276061>, 2010.
- Thoppil, P. G., Frolov, S., Rowley, C. D., Reynolds, C. A., Jacobs, G. A., Joseph Metzger, E., Hogan, P. J., Barton, N., Wallcraft, A. J., Smedstad, O. M., and Shriver, J. F.: Ensemble forecasting greatly expands the prediction horizon for ocean mesoscale variability, *Communications Earth and Environment*, 2, 89, <https://doi.org/10.1038/s43247-021-00151-5>, 2021.
- 865 Trodahl, M. and Isachsen, P. E.: Topographic Influence on Baroclinic Instability and the Mesoscale Eddy Field in the Northern North Atlantic Ocean and the Nordic Seas, *Journal of Physical Oceanography*, 48, 2593–2607, <https://doi.org/10.1175/JPO-D-17-0220.1>, 2018.
- Truesdell, C. and Noll, W.: The Non-Linear Field Theories of Mechanics, in: *The Non-Linear Field Theories of Mechanics*, edited by Truesdell, C., Noll, W., and Antman, S. S., pp. 57–73, Springer, Berlin, Heidelberg, https://doi.org/10.1007/978-3-662-10388-3_1, 2004.
- 870 van Sebille, E., Griffies, S. M., Abernathey, R., Adams, T. P., Berloff, P., Biastoch, A., Blanke, B., Chassignet, E. P., Cheng, Y., Cotter, C. J., Deleersnijder, E., Döös, K., Drake, H. F., Drijfhout, S., Gary, S. F., Heemink, A. W., Kjellsson, J., Koszalka, I. M., Lange, M., Lique, C., MacGilchrist, G. A., Marsh, R., Mayorga Adame, C. G., McAdam, R., Nencioli, F., Paris, C. B., Piggott, M. D., Polton, J. A., Rühls, S., Shah, S. H. A. M., Thomas, M. D., Wang, J., Wolfram, P. J., Zanna, L., and Zika, J. D.: Lagrangian ocean analysis: Fundamentals and practices, *Ocean Modelling*, 121, 49–75, <https://doi.org/10.1016/j.ocemod.2017.11.008>, 2018.

- 875 Wei, M., Jacobs, G., Rowley, C., Barron, C. N., Hogan, P., Spence, P., Smedstad, O. M., Martin, P., Muscarella, P., and Coelho, E.: The impact of initial spread calibration on the RELO ensemble and its application to Lagrangian dynamics, *Nonlinear Processes in Geophysics*, 20, 621–641, <https://doi.org/10.5194/npg-20-621-2013>, 2013.
- Wei, M., Jacobs, G., Rowley, C., Barron, C. N., Hogan, P., Spence, P., Smedstad, O. M., Martin, P., Muscarella, P., and Coelho, E.: The performance of the US Navy’s RELO ensemble, NCOM, HYCOM during the period of GLAD at-sea experiment in the Gulf of Mexico, *Deep Sea Research Part II: Topical Studies in Oceanography*, 129, 374–393, <https://doi.org/10.1016/j.dsr2.2013.09.002>, the Gulf of Mexico Ecosystem - before, during and after the Macondo Blowout, 2016.
- 880 Wilde, T., Rössl, C., and Theisel, H.: FTLE Ridge Lines for Long Integration Times, in: 2018 IEEE Scientific Visualization Conference (SciVis), pp. 57–61, <https://doi.org/10.1109/SciVis.2018.8823761>, 2018.
- Zhong, X., Wu, Y., Hannah, C., Li, S., and Niu, H.: Applying finite-time Lyapunov exponent to study the tidal dispersion on oil spill trajectory in Burrard Inlet, *Journal of Hazardous Materials*, 437, 129 404, <https://doi.org/10.1016/j.jhazmat.2022.129404>, 2022.
- 885 Zimmerman, J.: The tidal whirlpool: A review of horizontal dispersion by tidal and residual currents, *Netherlands Journal of Sea Research*, 20, 133–154, [https://doi.org/10.1016/0077-7579\(86\)90037-2](https://doi.org/10.1016/0077-7579(86)90037-2), 1986.
- Zimmermann, J., Motejat, M., Rössl, C., and Theisel, H.: FTLE for Flow Ensembles by Optimal Domain Displacement, arXiv e-prints, <https://arxiv.org/abs/2401.04153>, 2024.